

---

# Graph-based Unsupervised Disentangled Representation Learning via Multimodal Large Language Models

---

Baao Xie<sup>1</sup> Qiuyu Chen<sup>1,2</sup> Yunnan Wang<sup>1,2</sup> Zequn Zhang<sup>1,3</sup> Xin Jin<sup>1,\*</sup> Wenjun Zeng<sup>1</sup>

<sup>1</sup>Ningbo Institute of Digital Twin, Eastern Institute of Technology, Ningbo, China

<sup>2</sup>Shanghai Jiao Tong University, Shanghai, China

<sup>3</sup>University of Science and Technology of China, Hefei, China

bxie@idt.eitech.edu.cn jinxin@eitech.edu.cn

## Abstract

Disentangled representation learning (DRL) aims to identify and decompose underlying factors behind observations, thus facilitating data perception and generation. However, current DRL approaches often rely on the unrealistic assumption that semantic factors are statistically independent. In reality, these factors may exhibit correlations, which off-the-shelf solutions have yet to properly address. To tackle this challenge, we introduce a bidirectional weighted graph-based framework, to learn factorized attributes and their interrelations within complex data. Specifically, we propose a  $\beta$ -VAE based module to extract factors as the initial nodes of the graph, and leverage the multimodal large language model (MLLM) to discover and rank latent correlations, thereby updating the weighted edges. By integrating these complementary modules, our model successfully achieves fine-grained, practical and unsupervised disentanglement. Experiments demonstrate our method’s superior performance in disentanglement and reconstruction. Furthermore, the model inherits enhanced interpretability and generalizability from MLLMs.

## 1 Introduction

Disentangled representation learning (DRL) is a major goal of artificial intelligence (AI), acclaimed for its enhancement of model robustness, interpretability, and generalizability. Essentially, DRL methods imitate the understanding processes of biological intelligence, wherein comprehension of real-world is achieved by separating observations into distinct factors [1]. In this form, specific attributes (e.g., object color, shape, and size) exhibit exclusive sensitivity to the changes of specific factors. Learning of such disentangled representations is of great importance across various domains, e.g., computer vision [2, 3, 4, 5, 6], natural language processing [7, 8, 9], and AI generated content [10, 11, 12, 13]. In the current phase, unsupervised DRL methods primarily utilize the Variational Autoencoder (VAE) framework [14], a probabilistic model learning representations through a regularization term. This term involves the Kullback-Leibler divergence between the posterior distribution of latent factors and a standard multivariate Gaussian prior, thereby encouraging the factorized representations. To strengthen disentanglement, co-current research [15, 16, 17, 18] focus on the optimization and refinement of the original VAE regularizers, resulting in the family of VAE-based DRL approaches.

Despite the advanced results of the simple and synthetic datasets, VAE-based DRL methods still fall short in interpretability and robustness that are required for effective disentanglement in complex data [19]. This limitation mainly stems from the unrealistic assumption that underlying factors

---

\*Xin Jin is the corresponding author. Code is available at [here](#).

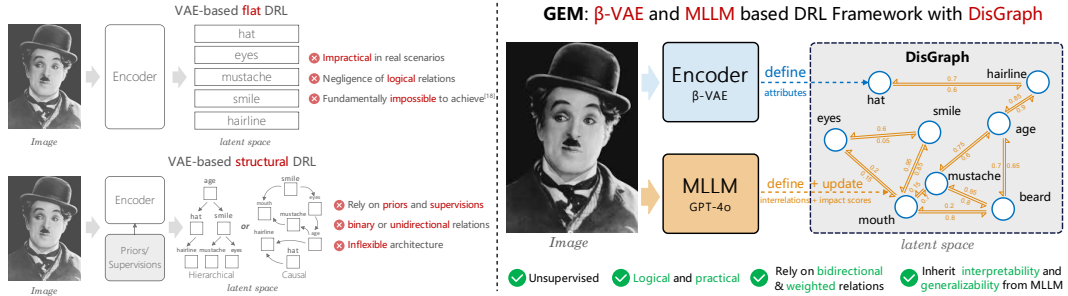


Figure 1: The comparison of typical DRL frameworks with our GEM. The limitations of conventional DRL methods are presented on the left. Conversely, the right-hand side illustrates the advantages of our framework, which benefited from the integration of the  $\beta$ -VAE and MLLMs.

are countable, independent, and can be fully disentangled in an unsupervised manner (refer to the top-left of Figure 1). In contrast, the real-world variables are pervasively correlated: red apples are more common than yellow ones; elderly people are more frequent with white hair and a receding hairline. Accordingly, an increasing number of recent studies [20, 21, 19, 22] showcases that purely unsupervised DRL is fundamentally impossible without extra priors and inductive biases.

The struggle of typical DRL methods on the complex data returns us back to the essential goal of DRL, i.e., understanding the world as biological intelligence does. This cognitive process can be naturally segmented into three phases: attribute extraction, interrelation perception, and knowledge combination [23, 24], where the latter two stages should not be neglected. From this perspective, several structured DRL approaches, typically known as Hierarchical DRL [25, 26, 12] and Causal DRL [21, 27, 28, 29], have involved the correlations between attributes. However, these approaches usually require extra supervision, and their relations are invariably represented by binary and unidirectional fusion, thus limiting the model performance in practical scenarios (refer to the bottom-left of Figure 1). Inspired by the analysis above, we argue that an effective and practical disentanglement framework should meet the following criteria: (i) the framework should be fully unsupervised; (ii) the framework should be able to disentangle factors while concurrently discovering logical interrelations among them; (iii) the interrelations should be modeled as bidirectional, with corresponding impact scores assigned to each, thereby improving model performance in complex scenarios. On this basis, we propose a novel Graph-based disEntanglement framework with Multimodal large language models, dubbed GEM. Specifically, our model employs two complementary branches: a  $\beta$ -VAE based disentanglement branch for the attribute extraction, and a multimodal large language model (MLLM) based branch for the interrelation discovery. The relation-aware representations are further embedded into a disentangled bidirectional weighted graph (DisGraph), which presents distinct factors as nodes, interrelations as edges, and impact scores as weights. The parameters of the graph are dynamically updated and refined via a graph learner. The experimental results show that GEM achieves superior performance on fine-grained and relation-aware disentanglement, while preserving the reconstruction quality. Furthermore, the model is endowed with superior interpretability and generalizability that derived from MLLMs. All in all, our main contributions can be summarised as:

- To our best knowledge, we are the first to leverage the commonsense reasoning of MLLMs to discover and rank the semantic interrelations from the perspective of DRL.
- We propose a novel and practical disentanglement framework built upon  $\beta$ -VAE and MLLMs to learn the independent factors and their interrelations in an unsupervised way.
- We introduce a bidirectional and self-driven graph architecture to encode the relation-aware representations, thus facilitating practical and controllable disentanglement.

## 2 Related Work

### 2.1 Standard Disentangled Representation Learning

The definition of DRL is intuitively given by Bengio et al. [1] as a technique to separate semantic factors behind observational data. This approach assumes that individual data attributes are sensitive to changes in single latent factors, while not being affected by other factors. The disentanglement of

attributes is believed helpful for downstream tasks, e.g., generative models [3, 30, 5, 31, 32], medical imaging [33, 34, 35], image editing [36, 37, 38, 39], and 3D reconstruction [40, 41, 42].

Traditional DRL methods primarily utilizes the VAE framework, achieving a measure of disentanglement on static datasets. This framework has been further enhanced by extensive models such as  $\beta$ -VAE [15],  $\beta$ -TCVAE [16], DIP-VAE [4], FactorVAE [43], RF-VAE [44], and  $\alpha$ -TCVAE [18] through the optimizations of regularization terms. Despite the successes on simple and static datasets, standard DRL approaches still encounter challenges in complex data. It is mainly due to the flat and unrealistic assumption: data properties are independent and can be factorized into distinct factors [1, 21, 45, 46]. Locatello et al. [20] have proven that unsupervised DRL is fundamentally impossible without extra priors. Thus, subsequent studies have demonstrated that a practical DRL model with appropriate inductive biases can enhance the disentanglement in real scenes [47, 48, 49, 50].

## 2.2 Structured Disentangled Representation Learning

In contrast to the flat and VAE-based DRL methods, recent research gradually realize that latent factors might naturally involve semantic interrelations, deriving to the branch of structured disentangled representation learning [19]. Within this domain, Hierarchical DRL and Causal DRL are mostly relevant to our work. Hierarchical DRL presumes that underlying factors have different levels of semantic abstraction, either dependent [51] or independent [25] across levels. While straightforward, Li et al. [25] propose a hierarchical VAE-based model to learn semantic representations. Furthermore, Singh et al. [12] introduce FineGAN, a three-tier hierarchical framework for controllable object generation. Li et al. [52] also propose a hierarchical DRL framework aimed at facilitating image-to-image translation. Differently, our framework aims to achieve fine-grained disentanglement, where the targeted attributes are always flat, e.g., the wrinkle, lipstick, and mustache of faces. Therefore, we rely on the flat representations, but place a strong emphasis on the mutual relations between attributes.

Similarly, Causal DRL methods endeavor to capture the causal relations between disentangled factors. As the first, Yang et al. [21] propose CausalVAE to discover relations from the perspective of causality. Further, Shen et al. [29] propose a weakly supervised framework DEAR with the structured causal model (SCM) as prior. However in our view, current Causal DRL methods have at least three unpractical issues: (i) rely on various degrees of supervision; (ii) aim to model a specific event rather than a common scenario; (iii) the causal relationship is often overly simplistic, being impractically binary and unidirectional, i.e., paired variables A and B only have two possible causal relations: either  $A \rightarrow B$  or  $A \leftarrow B$  (otherwise unrelated). In practical, it is common for paired variables to exhibit bidirectional influence, and the impact of such bidirectional relations should be properly ranked.

## 2.3 Multimodal Large Language Models

Recent years have witnessed the remarkable advancements in Multimodal Large Language Model (MLLM) [53, 54, 55, 56]. Since the release of Generative Pre-trained Transformer (GPT) [57], there has been a research trend over MLLMs regarding to its demonstrated potential in processing multimodal data [58, 59, 60]. As the variants of GPT-4, GPT-4 with Vision (GPT-4V) [61] and GPT-4 omni (GPT-4o) [62] enhance to process textual and visual data, enabling richer, context-aware interactions across a range of multimodalities. Concurrently, following works such as Gemini [58], Claude [63], NExT-GPTs [64] and GLM-4 [65] have strengthen the support to additional modalities.

The powerful capacities of MLLMs gradually make researchers aware of its latent perceptual knowledge embedded within networks. Gandelsman et al. [59] investigate the way that CLIP encoder understands visual data, by decomposing representations into individual components. In addition, Basu et al. [66] propose a mechanistic localization approach to explore how the visual properties are encoded in MLLMs. However, to our best knowledge, there is limited exploration into leveraging the commonsense reasoning of MLLMs from the perspective of DRL. And we are the first to employ MLLMs to discover and rank interrelations between semantic factors in the DRL framework.

## 3 Methodology

To achieve fine-grained and relation-aware disentanglement, we propose GEM, a novel and practical framework that synergizes the strengths of DRL and MLLMs by a bidirectional weighted DisGraph. As depicted in Figure 2, GEM is comprised of two complementary modules: a  $\beta$ -VAE based

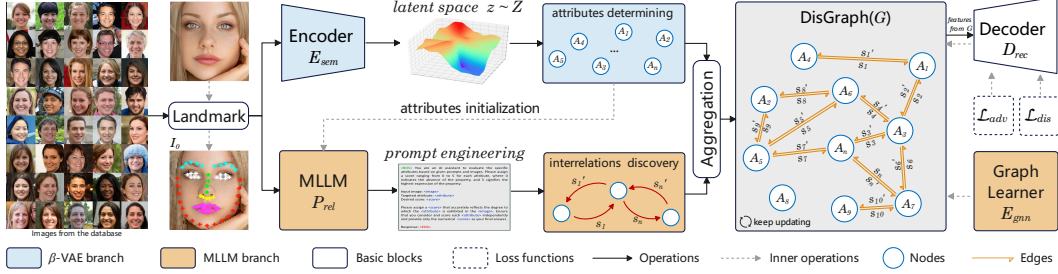


Figure 2: Pipeline of our GEM. The model consists of two complementary branches, termed as a  $\beta$ -VAE branch (blue) and a MLLM branch (brown). The former utilizes  $\beta$ -VAE based semantic encoder  $E_{sem}$  to disentangle underlying factors, while the latter employs prompt engineering to discover and rank interrelations. The bidirectional weighted DisGraph  $G$  is further proposed to embed relation-aware representations, with its parameters optimized constantly by a GNN network  $E_{gnn}$ .

branch dedicated to extract attributes (Section 3.1), and a MLLM-based branch to discover and rank interrelations (Section 3.2). The relation-aware representations are then embedded into the DisGraph (Section 3.3), which presents factors as nodes, interrelations as edges, and impact scores as weights.

### 3.1 $\beta$ -VAE based Attribute Determining Branch

The fundamental objective of vanilla VAE is to approximate data distributions by employing a maximum likelihood estimation framework as outlined in Eq. 1:

$$\log p_{\theta}(\mathbf{x}) = D_{KL}(q_{\phi}(\mathbf{z}|\mathbf{x})||p_{\theta}(\mathbf{z}|\mathbf{x})) + \mathcal{L}(\theta, \phi), \quad (1)$$

where the variational posterior distribution  $q_{\phi}(\mathbf{z}|\mathbf{x})$  is utilized to represent the probability distribution of the latent variable  $z$  given the observation  $x$ . The key of Eq. 1 is maximizing the approximation  $\log p_{\theta}(\mathbf{x})$  of the true posterior distribution  $p_{\theta}(\mathbf{z}|\mathbf{x})$  and  $q_{\phi}(\mathbf{z}|\mathbf{x})$ .

Specifically, the first term of Eq. 2 corresponds to the Kullback-Leibler (KL) divergence measuring the distance between distribution  $q_{\phi}(\mathbf{z}|\mathbf{x})$  and  $p_{\theta}(\mathbf{z}|\mathbf{x})$ . The second term is denoted as the variational evidence lower bound (ELBO). Empirically, the maximization of ELBO is employed to provide a stringent tight lower bound for the original log-likelihood  $\log p_{\theta}(\mathbf{x})$ . ELBO can be reformulated as:

$$\mathcal{L}(\theta, \phi) = \mathbb{E}_{q_{\phi}(\mathbf{z}|\mathbf{x})} [\log p_{\theta}(\mathbf{x}|\mathbf{z})] - \beta D_{KL}(q_{\phi}(\mathbf{z}|\mathbf{x})||p_{\theta}(\mathbf{z})), \quad (2)$$

where the initial term, i.e., conditional logarithmic likelihood  $\mathbb{E}_{q_{\phi}(\mathbf{z}|\mathbf{x})} [\log p_{\theta}(\mathbf{x}|\mathbf{z})]$  is responsible for the reconstruction. Typically, the latent variable  $z$  is assumed to follow a standard Gaussian distribution  $\mathcal{N}(0, 1)$  for  $p_{\theta}(z)$ , so that the KL term actually imposes independent constraints on the representations. Furthermore, subsequent studies [15, 17, 67] highlight that a extra penalty coefficient prior to the KL term, denoted by  $\beta$ , can significantly strengthen disentanglement. When  $\beta$  is set to 1, the  $\beta$ -VAE reverts to the standard VAE framework. And an increase in  $\beta$  encourages more disentangled representations but harms the performance of reconstruction as a trade-off. As per the Information Bottleneck (IB) theory [17], constraining the information input to DRL models (e.g., via  $\beta$  penalty coefficient) inherently enables them to identify and learn the most representative factors for successful reconstruction. For instance, when trained on the Shapes3D (a collection of synthetic objects) with a merely three-dimensional latent variable, the attribute determining branch tends to learn the most critical factors, observed to be "object color", "object shape", and "background shape". These attributes are organized in the three dimensions, ordered by their reconstruction contribution.

Specifically, within the processes of this branch, the input image is firstly subjected to a pre-processing step utilizing landmark detection functions as instructed by [68] and [69] (see Figure 2). It serves as a regularization phase, to remain the key features through targeted cropping. Additional derivations of this process are documented in the appendix. Then, the pre-processed  $I_0$  is fed into a  $\beta$ -VAE based branch, designed to disentangle factors associated with each dimension in the latent variable  $z \in Z$ . However, the input of decoder  $D_{rec}$  is the relation-aware variable  $z_{rel} = \mathbf{A}^T z$  from the DisGraph, rather than the  $z \in Z$ . It means the prior assumption of  $p_{\theta}(z) \in \mathcal{N}(0, 1)$  is no longer hold. To address this issue, we reformulate the loss function in  $\beta$ -VAE as follows:

$$L_{gem}(\phi, \gamma, \theta) = D_{KL}(q_{\phi}(x, z), p_{\gamma, \theta}(x, z)) \quad (3)$$

$$\nabla_{\theta} L_{gem}(\phi, \gamma, \theta) \stackrel{x=D_{\theta}(z)}{=} -E_{z \sim q(z)} \nabla_x \left[ \log \left( \frac{p_{\theta, \gamma}(x, z)}{q_{\phi}(x, z)} \right) \right] \nabla_{\theta} x \quad (4)$$



$$\nabla_{\phi} L_{gem}(\phi, \gamma, \theta) \stackrel{z=E_{\phi}(x)}{=} E_{x \sim p(x)} \nabla_z \left[ \log \left( \frac{p_{\theta, \gamma}(x, z)}{q_{\phi}(x, z)} \right) \right] \nabla_{\phi} z \quad (5)$$

$$\nabla_{\gamma} L_{gem}(\phi, \gamma, \theta) \stackrel{z=G_{\gamma}(z)}{=} E_{x \sim p(x)} \nabla_z \left[ \log \left( \frac{p_{\theta, \gamma}(x, z)}{q_{\phi}(x, z)} \right) \right] \nabla_{\gamma} z \quad (6)$$

where the  $\phi$ ,  $\theta$  and  $\gamma$  are the learnable parameters of  $E_{sem}$ ,  $D_{rec}$  and DisGraph  $G$ , respectively. Let's say  $D(x, y) = \log \left( \frac{p_{\theta}(x, z)}{\beta q_{\phi}(x, z)} \right)$ , and the the gradients with respect to  $x$  and  $z$  can be obtained during backpropagation by the cross-entropy:

$$\mathcal{L}_{adv} = \mathcal{L}_{D(x, y)} = \frac{1}{N_{bc} N_m} \left[ \sum_{i=0}^{N_{bc}} \text{softplus}(-D(x_i, z_i)) + \sum_{i=0}^{N_{bc}} \text{softplus}(D(x_i, z_i)) \right] \quad (7)$$

where  $N_{bc}$  and  $N_m$  represent the number of samples and the posterior samples in a batch, respectively. Obviously, this loss resembles the adversarial loss utilized in Generative Adversarial Networks (GAN) [70]. Therefore, we employ the adversarial training strategy to optimize  $D(x, y)$ . Combined with the disentanglement term from the original  $\beta$ -VAE indicated as  $\mathcal{L}_{dis}$ , the total loss for the attribute determining branch can be expressed as:

$$\mathcal{L}_{total} = \lambda_{adv} \mathcal{L}_{adv} + \lambda_{dis} \mathcal{L}_{dis} + \lambda_{gem} \mathcal{L}_{gem} \quad (8)$$

where the  $\lambda_{adv}$ ,  $\lambda_{dis}$  and  $\lambda_{gem}$  serve as hyperparameters to balance the disentanglement capability and reconstruction quality, with default values set to 0.8, 0.6 and 0.6, respectively. The detailed derivation process of the adversarial training strategy is provided in the supplementary material.

### 3.2 MLLM-based Interrelation Discovery Branch

Given a pre-processed image  $I_0$  with  $n$  targeted attributes  $\mathcal{A} = \{1, 2, 3, \dots, n\}$  initialized by the  $\beta$ -VAE branch, our objective is to discover and rank the mutual relations for each pair within  $\mathcal{A}$ . As represented by the brown blocks in Figure 2, we employ MLLMs as a relation predictor  $P_{rel}$  to discover and rank interrelations. Initially, the MLLM is required to score from 0 to 5 for each attribute, where 0 indicates the attribute's absence, and 5 denotes its highest expression. As shown in Figure 3, the queries can be formulated as a question in natural language with the input image  $I_0$ .

Based on the attribute scores, we subsequently employ Somers' D algorithm [71] to rank the bidirectional impact scores of interrelations. For the attribute pair  $(A_i, A_j)$ , we determine the number of concordant pairs  $N_C$  and discordant pairs  $N_D$ , as delineated by Kendall's Tau [72] algorithm. Subsequently, the impact score  $\mathcal{S}_{ij}$  within  $\mathcal{S} = \{1, 2, 3, \dots, k\}$  can be denoted as:

$$\mathcal{S}_{ij} = \frac{N_c - N_d}{N_c + N_d + T_i} \quad (9)$$

For the reversed relation of  $(A_i, A_j)$ , the impact score can be denoted as  $\mathcal{S}_{ji}$  or  $\mathcal{S}'_{ij}$ :

$$\mathcal{S}'_{ij} = \mathcal{S}_{ji} = \frac{N_c - N_d}{N_c + N_d + T_j} \quad (10)$$

where  $T_i$  and  $T_j$  is the number of ties only for the independent variable  $A_i$  and  $A_j$ , respectively. The calculated  $\mathcal{S}$  and  $\mathcal{S}'$  are used for initialization and refinement of DisGraph (see Section 3.3). As illustrated in Figure 4, it is important to clarify that the primary goal of the MLLM branch in GEM is to discover interrelations, where the statistical relativity between two attributes is of primary concern, rather than the absolute scores for the individual attribute. For example, given a collection of facial images, it is acceptable if the scores of "age" and "bald" exhibit a positive correlation, even if the specific score values are fluctuating. To ascertain the reliability of MLLMs for interrelation discovery, extra experiments are performed as shown in Section 4.4.

<BOS> You are an AI assistant to evaluate the specific attributes based on given prompts and images. Please assign a score ranging from 0 to 5 for each attribute, where 0 indicates the absence of the attribute, and 5 signifies the highest expression of the attribute.

Input image: <image>  
Targeted attribute: <attribute>  
Desired degree score: <score>

.....

Please assign a <score> that accurately reflects the expressive level to which the <attribute> is exhibited in the <image>. Ensure that you consider and score each <attribute> independently and provide only the numerical <score> score as your final answer.

Response: <EOS>

Figure 3: A simplified example of the template for prompting MLLMs to evaluate attributes. Specifically, <text> is the interactive token, while <BOS> and <EOS> are tokens denoting the start and end of the input to MLLMs, respectively.

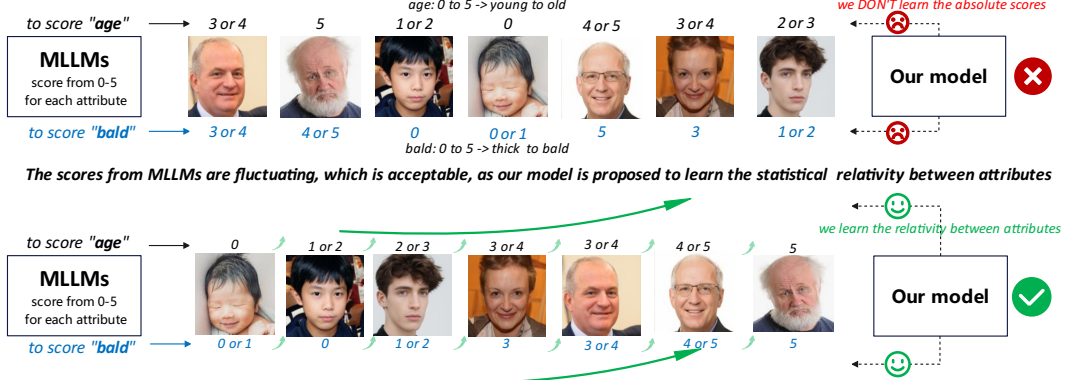


Figure 4: Our aim is using the commonsense knowledge behind MLLMs to equip GEM with ability of interrelations discovery, where a certain degree of fluctuations on absolute scores are acceptable.

### 3.3 Bidirectional Weighted DisGraph

Based on the extracted factors and interrelations, we then propose the bidirectional weighted DisGraph  $\mathcal{G} = (\mathcal{A}, \mathcal{E}, \mathcal{S})$  to integrate the semantic representations. Specifically,  $\mathcal{A}$  is the set of  $n = |\mathcal{A}|$  nodes, embodying the disentangled attributes as factors. Besides,  $\mathcal{E}$  is the set of  $k = |\mathcal{E}|$  edges, and  $\mathcal{S}$  stands for the weights of these edges. An  $e \in \mathcal{E}$  and its corresponding impact score  $s \in \mathcal{S}$  are embedded. Consequently,  $\mathcal{G}$  can be presented as the learnable weighted adjacency matrix  $\mathbf{A} \in [0, 1]^{n \times n}$ .

According to the definitions above, the model firstly constructs a sketched adjacency matrix  $\mathbf{A}_0 \in \mathbb{R}^{n \times n}$  upon the factors and relations initialized by the  $\beta$ -VAE branch and MLLM branch. Specifically, we treat the averaged impact scores of the first 1,500 images processed by MLLMs, as initial weights of relations. We further employ an unsupervised graph learner  $E_{gnn}$  to dynamically refine the parameters of DisGraph by the structure bootstrapping mechanism [73] and multi-view graph contrastive learning [74]. The optimization function of  $E_{gnn}$  can be formulated as:

$$\mathbf{T}^{(l)} = h_w^{(l)}(\mathbf{T}^{(l-1)}, \mathbf{A}) = \sigma\left(\tilde{\mathbf{D}}^{-\frac{1}{2}} \tilde{\mathbf{A}} \tilde{\mathbf{D}}^{-\frac{1}{2}} \mathbf{T}^{(l-1)} \Omega^{(l)}\right), \quad (11)$$

It converts the sketched adjacency matrix  $\mathbf{A}_0$  into node embedding  $\mathbf{T}$  via the GNN-based multilayer network, where  $h_w^{(l)}(\cdot)$  is the embedding function with learnable parameters  $w$  of the  $l$ -th layer and  $\mathbf{T}^{(l)}$  is the output matrix. The augmented adjacency matrix  $\tilde{\mathbf{A}} = \mathbf{A} + \mathbf{I}$  incorporates self-loops based on the initial matrix  $\mathbf{A}_0$ , and  $\tilde{\mathbf{D}}$  is the degree matrix of  $\tilde{\mathbf{A}}$ . Further,  $w^{(l)} = \Omega^{(l)} \in \mathbb{R}^{n \times n}$  denotes the parameter matrix of the  $l$ -th layer, with  $\sigma(\cdot)$  as a non-linear function that enhances training stability.

Figure 5 illustrates the comprehensive training algorithm of our model. The encoder processes input images and outputs the disentangled latent variable  $z$ , which subsequently initializes the embeddings of nodes in DisGraph. The adjacency matrix of DisGraph is calculated using Somer's D algorithm, which processes the attribute scores outputted by the MLLM. Following this initialization, a Graph Neural Network (GNN) refines the structure of DisGraph. The average of the feature matrix within DisGraph is then forwarded to the decoder to reconstruct images. Concurrently, the discriminator is trained to approximate the gradient of the loss function. Assuming that the model's performance is upper bounded by the norm of its gradient, which satisfies the Polyak-Lojasiewicz (PL) condition, this configuration ensures the suboptimality of the model.

Algorithm 1: Training Algorithm of GEM

---

**Input:** Image dataset  $X$ , Encoder  $E_{sem}$ , DisGraph  $G$ , Decoder  $D_{rec}$ , Discriminator  $D$ , parameters of the encoder  $E_{sem}$ , DisGraph  $G$  decoder  $D_{rec}$  and Discriminator  $D$  are denoted as  $\phi, \gamma, \theta$  and  $\alpha$

**Output:** Disentangled latent variable  $z \in \mathbb{R}^{pre}$ , Correlation-involved latent variable  $z_{rel} \in \mathbb{R}^{pre}$ , reconstructed image  $\hat{x}$

---

```

1 while  $i \leq N$  do
2    $att_i = MLLM(x_i)$ ; // Getting the attribute scores by MLLM
3 end
4  $A_{adj} \leftarrow SomersD(att)$ ; // Getting adjacency matrix by Somer's D algorithm
5 while  $i \leq T$  do
6    $z = E_{sem}(x_i)$ ;
7   embeddings[i]  $\leftarrow$  Mask( $z, i$ );
8   embeddings  $\leftarrow$  G( $A_{adj}, embeddings$ );
9   // Refine the DisGraph by using GNN
10   $z_{rel} \leftarrow \frac{1}{N_{node}} \sum_i embeddings[i]$ ;
11   $\hat{x} = D(z_{rel})$ ;
12  Calculate  $L_{gem}, L_{dis}$  and  $L_{adv}$ ;
13   $\theta \leftarrow \theta - \eta_1 \nabla_{\theta} L_{gem}(\phi, \gamma, \theta) - \eta_2 \nabla_{\phi} L_{dis}(\phi, \theta)$ ;
14   $\phi \leftarrow \phi - \eta_1 \nabla_{\phi} L_{gem}(\phi, \gamma, \theta) - \eta_2 \nabla_{\phi} L_{dis}(\phi, \theta)$ ;
15   $\gamma \leftarrow \gamma - \eta_3 \nabla_{\gamma} L_{gem}(\phi, \gamma, \theta)$ ;
16   $\alpha \leftarrow \alpha - \eta_4 \nabla_{\alpha} L_{adv}(\alpha)$ ;
17   $i = i + 1$ ;
18 end
```

---

Figure 5: Overall training algorithm of GEM.

Assuming that the model's performance is upper bounded by the norm of its gradient, which satisfies the Polyak-Lojasiewicz (PL) condition, this configuration ensures the suboptimality of the model.

## 4 Experiments

**Datasets.** We evaluate the GEM on two datasets: 1) **CelebA** [75] contains over 200,000 high-quality facial images. Each image is annotated with 40 binary attribute labels, making it a widely used benchmark for supervised DRL methodologies. Operating in an unsupervised manner, we do not utilize ground-truth labels from this dataset, yet we still conduct comparisons against the supervised approaches; 2) **LSUN** [76] consists of about one million images across various object categories such as cars, buildings, animals, etc. We select a typical subset from both scene categories and object categories, as bedroom and horse, respectively. We believe these two datasets are diverse enough to assess our method covering complex data of different object types.

**Implementation details.** We implement GEM with PyTorch [77]. The landmark pre-processing settings follow the instructions of [68] and [69]. In addition, we employ the latest GPT-4o [62] as the interrelation predictor. For every experiment, the latent dimension size is set to 6. Concentrating on the disentanglement capacity of the framework, all experimental images are resized to a resolution of  $64 \times 64$  to minimize computational resources. For high-definition outcomes at  $256 \times 256$ , refer to Appendix A.7. All the experiments are processed using the Adam optimizer with a learning rate of  $1e-4$ , and conducted on the Nvidia Tesla A100 GPUs, with a batch size of 32.

**Baselines for Comparison.** We evaluate the GEM with state-of-the-art DRL methods on the disentanglement capacity, reconstruction quality, and computational efficiency. The comparison encompasses supervised and unsupervised models, including standard VAE [14],  $\beta$ -VAE [15],  $\beta$ -TCVAE [16], FactorVAE [43] and DEAR [29]. All baselines are trained using the complete CelebA dataset under the configurations previously specified.

### 4.1 Qualitative Results

To evaluate the GEM’s effectiveness of relation-aware and fine-grained disentanglement, we perform qualitative analyses with FactorVAE [43] and DEAR [29]. The experiments are conducted on CelebA, a standard benchmark that has been previously validated as compatible with these methods. We select the six fine-grained facial attributes from the database including *Bangs*, *Bald*, *Gender*, *Beard*, *Blond*, and *Makeup*. The disentanglement results are represented by traversals across various latent dimensions, where each dimension corresponds to distinct attributes.

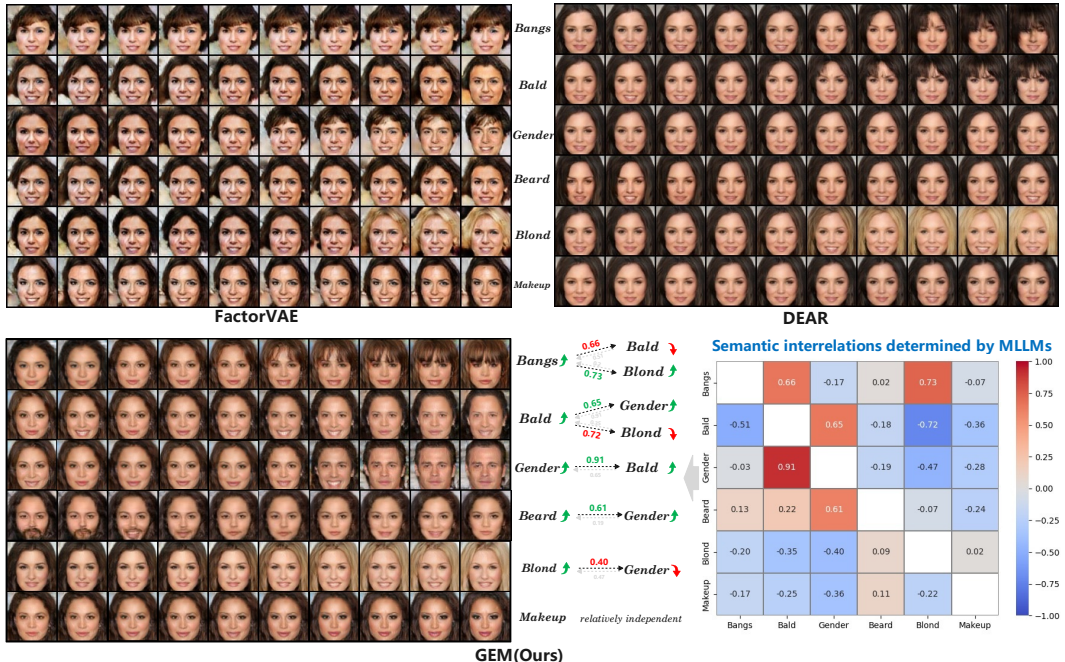


Figure 6: Qualitative comparisons between GEM and typical DRL Methods. Each row in facial images corresponds to the traversal on a specific attribute, as indicated adjacent to the images (i.e. *Bangs*, *Bald*, *Gender*, *Beard*, *Blond*, and *Makeup*). GEM exhibits superior ability in fine-grained disentanglement with discovered practical and bidirectional relations (illustrated by the heatmap).

As illustrated in Figure 6, GEM effectively achieves fine-grained and relation-aware disentanglement, via the integration of DRL and MLLMs. The interrelations determined by MLLMs are depicted as a heatmap in the bottom-right of Figure 6, where deeper colors reflect stronger relations. Since DisGraph is bidirectional, the impact scores for bidirectional relations between a pair of attributes may vary, resulting in an asymmetric matrix. Specifically, in the first row of GEM’s result, a person with heavier *Bangs* is less likely to be *Bald*, and the hair tends to be *Blond*, which is considered logical by MLLMs. Furthermore, as shown in the second and third rows, males (*Gender*) are more likely to be *Bald* and less likely to have *Blond* hair. The attribute *Makeup* is considered as relatively independent, with lower impacts scores among other attributes.

In comparison, DEAR demonstrates limitations in learning specific attributes such as *Bald* (second row) and *Gender* (third row), while the relations between attributes appear to be tenuous. To our knowledge, this underperformance may stem from the stringent nature of causal relations, which are single-directional and heavily rely on the quality of prior. For FactorVAE, since it is a flat DRL framework, we employ the same causal relations used in DEAR to make it relation-aware. As shown in Figure 4, GEM surpasses FactorVAE in both attribute disentanglement and relation discovery, which indicates the importance of specially-designed modules within our framework.

## 4.2 Quantitative Results

Table 1 reports the results of Frechet Inception Distance (FID) [70] and Kernal Inception Distance (KID) [70] scores to verify the quality of reconstructed images. To ensure statistical significance, each comparison model undergoes three rounds of evaluations in the same configuration. The results indicate that GEM outperforms both typical unsupervised (VAE,  $\beta$ -VAE,  $\beta$ -TCVAE, FactorVAE) and supervised approaches (DEAR) in terms of reconstruction quality. To our understanding, this superior performance is attributed to the specialized training strategy implemented in the framework.

Table 1: Quantitative comparison results with typical DRL approaches in FID and KID.

Method	CelebA		LSUN-horse		LSUN-bedroom	
	FID ↓	KID $\times 10^3$ ↓	FID ↓	KID $\times 10^3$ ↓	FID ↓	KID $\times 10^3$ ↓
VAE [15]	53.3 $\pm$ 0.6	51.4 $\pm$ 0.4	172.8 $\pm$ 1.7	181.7 $\pm$ 2.1	195.8 $\pm$ 4.1	226.4 $\pm$ 5.4
$\beta$ -VAE [15]	136.2 $\pm$ 1.6	107.0 $\pm$ 2.7	272.4 $\pm$ 3.2	294.2 $\pm$ 5.3	288.1 $\pm$ 5.7	225.7 $\pm$ 6.0
$\beta$ -TCVAE [16]	139.1 $\pm$ 0.8	113.2 $\pm$ 4.1	173.0 $\pm$ 4.8	217.35 $\pm$ 9.2	191.0 $\pm$ 5.0	179.2 $\pm$ 7.4
FactorVAE [43]	134.5 $\pm$ 0.3	92.0 $\pm$ 0.5	248.5 $\pm$ 5.5	155.3 $\pm$ 3.7	235.7 $\pm$ 3.2	172.8 $\pm$ 3.9
DEAR [29]	70.7 $\pm$ 0.3	52.6 $\pm$ 0.1	136.4 $\pm$ 1.6	113.7 $\pm$ 0.9	177.6 $\pm$ 3.5	157.8 $\pm$ 2.3
<b>GEM (Ours)</b>	<b>46.0 <math>\pm</math> 0.1</b>	<b>48.3 <math>\pm</math> 0.2</b>	<b>101.0 <math>\pm</math> 1.1</b>	<b>65.5 <math>\pm</math> 1.7</b>	<b>125.4 <math>\pm</math> 1.2</b>	<b>76.1 <math>\pm</math> 1.1</b>

As shown in Table 1, GEM surpasses baseline models in reconstruction quality on the datasets of CelebA, LSUN-horse, and LSUN-bedroom. However, the use of the disentanglement coefficient in the  $\beta$ -VAE branch leads to an inevitable trade-off in reconstruction quality, making the model less comparable to the models focused on generation quality (e.g., GAN and Diffusion [78]). Therefore, the integration with leading generative models can be a direction for our future work. For additional comparison results, please refer to Appendix A.1.

Table 2: Computational efficiency report in parameters size, FLOPs, memory cost and training time.

Models	Params(M)	GFLOPs(B)	Mem(M)	TT(s)
FactorVAE	55.9	3.8	200.5	63.9
DEAR	53.4	3.5	267.2	91.8
GEM (Single)	44.7	2.8	173.6	51.5
<b>GEM (Full)</b>	49.6	3.2	222.8	78.9

Furthermore, we evaluate four relation-aware models: FactorVAE, DEAR, GEM (Single), and GEM (Full), on quantitative comparisons of computational resources. Notably, GEM (Single) is the variant of GEM that incorporates single attribute determination branch (we only provide the initial relations to make it relation-aware). Table 2 shows that GEM outperforms DEAR and is comparable to FactorVAE on computational efficiency. This is mainly attributed to FactorVAE’s utilization of a simple convolutional encoder, whereas GEM employs a  $\beta$ -VAE based encoder to strengthen disentanglement. In addition, the efficiency of full GEM is slightly inferior to GEM (Single), due to the extra modules for relation discovery and refinement.



### 4.3 Evaluations of Interpretability and Generalizability

As a by-product, GEM inherits the interpretability and generalizability of MLLMs. Theoretically, owing to the commonsense reasoning faculties of MLLMs, our model can be generalized to discover any attributes and interrelations across various real-world objects and scenes. To demonstrate the robustness and generalizability of GEM, we perform extra experiments on more complex scenes in LSUN, specifically targeting the typical object subset LSUN-horse and the scene subset LSUN-bedroom. Furthermore, we test the attributes beyond the 40 specified in CelebA, collectively showcasing the model’s superiority. To highlight the characteristics of bidirectional weighted DisGragh, we intentionally select paired fine-grained attributes exhibiting inconsistent bidirectional relations.

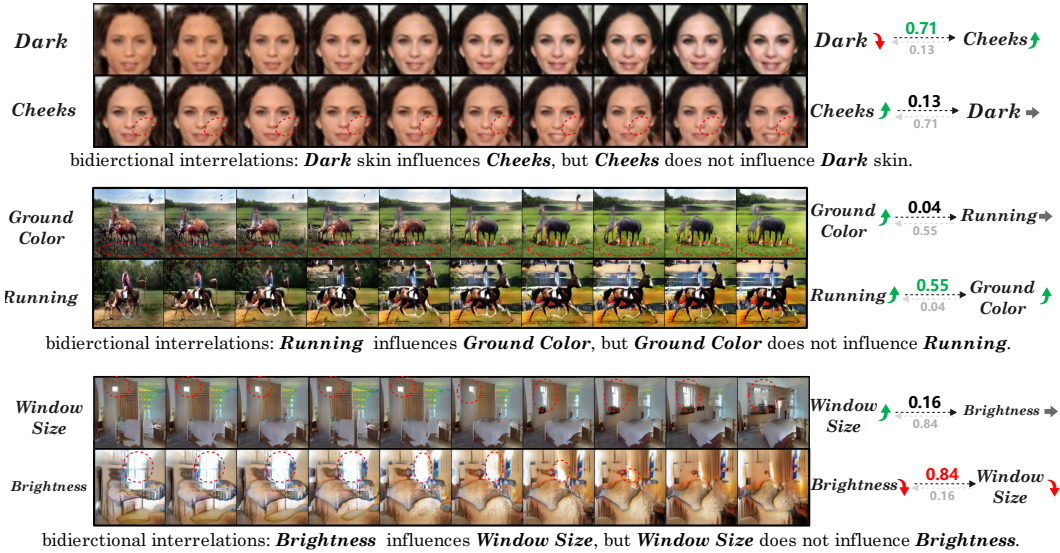


Figure 7: Relation-aware disentanglement results on LSUN and the attributes beyond CelebA. Paired fine-grained attributes with inconsistent bidirectional relations are chosen to indicate effectiveness.

As depicted in Figure 7, GEM successfully achieve fine-grained disentanglement on complex scenes, while identifying bidirectional and weighted relations among attributes. Furthermore, the artifacts observed in the results of LSUN datasets are mainly due to the datasets’ clutter (evidenced by the increase of FID and KID scores in Table 1). Nonetheless, despite the ambiguous and challenging nature of the data, GEM still obtain commendable disentanglement outcomes, affirming its robustness.

### 4.4 Evaluations of MLLMs

Our model leverages the commonsense knowledge embedded in MLLMs to predict interrelations. This is predicated on the assumption that MLLMs, including their future iterations, are powerful and reliable enough to comprehend the physical rules of the real world (e.g., aging brings wrinkles, sunrise brings light, etc.). Therefore, before utilizing the interrelation discovery branch, it is imperative to evaluate the reliability of MLLMs. This evaluation guarantees that the identified interrelations and their associated impact scores are dependable and can be effectively applied to downstream modules. To this purpose, we evaluate three latest MLLMs including GPT-4o, GPT-4v and GLM-4—against the ground truth attributes of the CelebA dataset. The horizontal axis presents the targeted attributes selected from the CelebA, where the vertical axis presents the percentage of scoring accuracy.

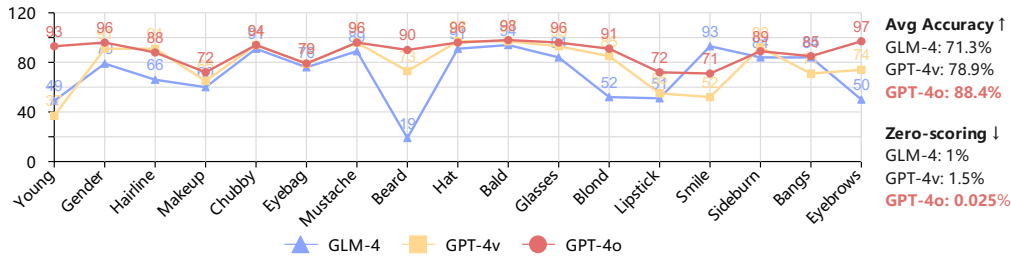


Figure 8: Evaluation experiments on the various MLLMs for attributes scoring.



As reported in Figure 8, GPT-4o outperforms other models on individual attribute scoring, achieving accuracy exceeding 90% for the majority of attributes. Specifically, it exhibits superior performance on attributes like *Beard*, *Young*, and *Eyebrows*, where other models yield significantly lower scores. In addition, GPT-4o achieves the highest average accuracy of 88.4% and the lowest zero-scoring rate at 0.25%, indicating a minimal rate of the meaningless predictions where all attributes are scored as zero. We conducted further evaluations on individual attributes, where GPT-4o also demonstrated superior performance (see Appendix A.7). Based on the evaluations, we employ GPT-4o as the interrelation predictor in the model.

#### 4.5 Ablation Study

To analyze the effectiveness of individual components in GEM, we perform an ablation study focusing on the importance of the  $\beta$ -VAE based branch, GNN-based graph learner  $E_{gmn}$ , and adversarial training strategy. The CelebA dataset served as the experimental platform for the investigations. It is worth noting that the complete removal of  $\beta$ -VAE branch is infeasible, as it would prevent the model from extracting attributes. Therefore to evaluate the importance of independent attribute extraction, we replace the  $\beta$ -VAE with the vanilla VAE, which does not enforce the independence of factors.

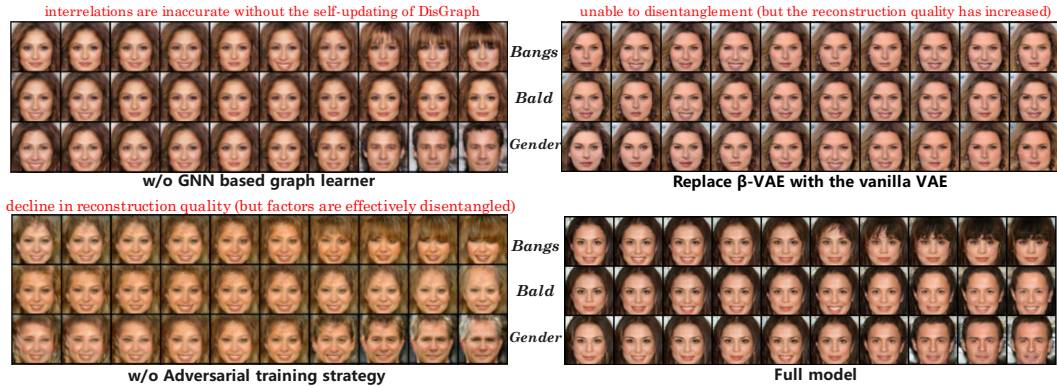


Figure 9: Ablation on replacing  $\beta$ -VAE with VAE, w/o graph learner, and w/o adversarial strategy.

As depicted in Figure 9, replacing  $\beta$ -VAE encoder results in a declined disentanglement capability, albeit with an improvement in reconstruction quality. In addition, the removal of GNN-based graph learner prevents the parameter updating of DisGraph, leading to the inaccurate determination of relations (e.g., the relation between *Bald* and *Gender* weakens). It is worth noting that the removal of both graph learner and initialization process within the framework precludes the learning of interrelations. Furthermore, eliminating the adversarial training strategy in GEM and relying solely on the standard VAE loss function results in a significant decline in reconstruction quality. The aforementioned results highlight the effectiveness of each part of our framework.

## 5 Conclusion

In this paper, we aim to explore the logical interrelations between semantic attributes within complex data, which is a critical challenge that existing DRL have yet to properly address. To this end, we introduce GEM, a  $\beta$ -VAE and MLLMs-based framework, designed to achieve fine-grained and relation-aware disentanglement. In this framework, DRL and MLLMs are integrated via a bidirectional and self-driven graph. Both qualitative and quantitative experiments demonstrate GEM’s superior disentanglement and reconstruction capacities over typical DRL models. In addition, the model shows its enhanced interpretability and generalizability inherited from MLLMs.

## 6 Acknowledgments

This research is supported by the IDT Foundation of Youth Doctoral Innovation [Grant S203.2.01.32.002], the National Natural Science Foundation of China [Grant 62302246] and the Zhejiang Provincial Natural Science Foundation of China [Grant LQ23F010008].

## References

- [1] Yoshua Bengio, Aaron Courville, and Pascal Vincent. Representation learning: A review and new perspectives. *IEEE transactions on pattern analysis and machine intelligence*, 35(8):1798–1828, 2013.
- [2] Luan Tran, Xi Yin, and Xiaoming Liu. Disentangled representation learning gan for pose-invariant face recognition. In *Proceedings of the IEEE conference on computer vision and pattern recognition*, pages 1415–1424, 2017.
- [3] Mingi Kwon, Jaeseok Jeong, and Youngjung Uh. Diffusion models already have a semantic latent space. *arXiv preprint arXiv:2210.10960*, 2022.
- [4] Abhishek Kumar, Prasanna Sattigeri, and Avinash Balakrishnan. Variational inference of disentangled latent concepts from unlabeled observations. *arXiv preprint arXiv:1711.00848*, 2017.
- [5] Andrey Voynov and Artem Babenko. Unsupervised discovery of interpretable directions in the gan latent space. In *International conference on machine learning*, pages 9786–9796. PMLR, 2020.
- [6] Dingkun Liu, Hongjie Zhou, Yilu Qu, Huimei Zhang, and Yongdong Xu. Umman: Unsupervised multi-graph merge adversarial network for disease prediction based on intestinal flora. *arXiv preprint arXiv:2407.21714*, 2024.
- [7] Pengyu Cheng, Martin Renqiang Min, Dinghan Shen, Christopher Malon, Yizhe Zhang, Yitong Li, and Lawrence Carin. Improving disentangled text representation learning with information-theoretic guidance. *arXiv preprint arXiv:2006.00693*, 2020.
- [8] Zhenya Huang, Xin Lin, Hao Wang, Qi Liu, Enhong Chen, Jianhui Ma, Yu Su, and Wei Tong. Disenqnet: Disentangled representation learning for educational questions. In *Proceedings of the 27th ACM SIGKDD Conference on Knowledge Discovery & Data Mining*, pages 696–704, 2021.
- [9] Giangiacomo Mercatali and André Freitas. Disentangling generative factors in natural language with discrete variational autoencoders. *arXiv preprint arXiv:2109.07169*, 2021.
- [10] Xi Chen, Yan Duan, Rein Houthoofd, John Schulman, Ilya Sutskever, and Pieter Abbeel. Infogan: Interpretable representation learning by information maximizing generative adversarial nets. *Advances in neural information processing systems*, 29, 2016.
- [11] Hong Chen, Yipeng Zhang, Xin Wang, Xuguang Duan, Yuwei Zhou, and Wenwu Zhu. Disenbooth: Disentangled parameter-efficient tuning for subject-driven text-to-image generation. *arXiv preprint arXiv:2305.03374*, 2023.
- [12] Krishna Kumar Singh, Utkarsh Ojha, and Yong Jae Lee. Finegan: Unsupervised hierarchical disentanglement for fine-grained object generation and discovery. In *Proceedings of the IEEE/CVF conference on computer vision and pattern recognition*, pages 6490–6499, 2019.
- [13] Yutong Hu, Yang Tan, Andi Han, Lirong Zheng, Liang Hong, and Bingxin Zhou. Secondary structure-guided novel protein sequence generation with latent graph diffusion. *arXiv preprint arXiv:2407.07443*, 2024.
- [14] Diederik P Kingma and Max Welling. Auto-encoding variational bayes. *arXiv preprint arXiv:1312.6114*, 2013.
- [15] Irina Higgins, Loic Matthey, Arka Pal, Christopher P Burgess, Xavier Glorot, Matthew M Botvinick, Shakir Mohamed, and Alexander Lerchner. beta-vae: Learning basic visual concepts with a constrained variational framework. *ICLR (Poster)*, 3, 2017.
- [16] Ricky TQ Chen, Xuechen Li, Roger B Grosse, and David K Duvenaud. Isolating sources of disentanglement in variational autoencoders. *Advances in neural information processing systems*, 31, 2018.
- [17] Christopher P Burgess, Irina Higgins, Arka Pal, Loic Matthey, Nick Watters, Guillaume Desjardins, and Alexander Lerchner. Understanding disentangling in  $\beta$ -vae. *arXiv preprint arXiv:1804.03599*, 2018.
- [18] Cristian Meo, Louis Mahon, Anirudh Goyal, and Justin Dauwels.  $\beta$ -tc-vae: On the relationship between disentanglement and diversity. In *The Twelfth International Conference on Learning Representations*, 2023.
- [19] Xin Wang, Hong Chen, Si’ao Tang, Zihao Wu, and Wenwu Zhu. Disentangled representation learning. *arXiv preprint arXiv:2211.11695*, 2022.

- [20] Francesco Locatello, Stefan Bauer, Mario Lucic, Gunnar Raetsch, Sylvain Gelly, Bernhard Schölkopf, and Olivier Bachem. Challenging common assumptions in the unsupervised learning of disentangled representations. In *international conference on machine learning*, pages 4114–4124. PMLR, 2019.
- [21] Mengyue Yang, Furui Liu, Zhitang Chen, Xinwei Shen, Jianye Hao, and Jun Wang. Causalvae: Disentangled representation learning via neural structural causal models. In *Proceedings of the IEEE/CVF conference on computer vision and pattern recognition*, pages 9593–9602, 2021.
- [22] Xingyi Yang, Jingwen Ye, and Xinchao Wang. Factorizing knowledge in neural networks. In *European Conference on Computer Vision*, pages 73–91. Springer, 2022.
- [23] Saeed Amizadeh, Hamid Palangi, Alex Polozov, Yichen Huang, and Kazuhito Koishida. Neuro-symbolic visual reasoning: Disentangling. In *International Conference on Machine Learning*, pages 279–290. Pmlr, 2020.
- [24] Tameem Adel, Han Zhao, and Richard E Turner. Continual learning with adaptive weights (claw). *arXiv preprint arXiv:1911.09514*, 2019.
- [25] Zhiyuan Li, Jaideep Vitthal Murkute, Prashna Kumar Gyawali, and Linwei Wang. Progressive learning and disentanglement of hierarchical representations. *arXiv preprint arXiv:2002.10549*, 2020.
- [26] Bin Tong, Chao Wang, Martin Klinkigt, Yoshiyuki Kobayashi, and Yuuichi Nonaka. Hierarchical disentanglement of discriminative latent features for zero-shot learning. In *Proceedings of the IEEE/CVF conference on computer vision and pattern recognition*, pages 11467–11476, 2019.
- [27] Pengzhou Wu and Kenji Fukumizu.  $\beta$ -intact-vae: Identifying and estimating causal effects under limited overlap. *arXiv preprint arXiv:2110.05225*, 2021.
- [28] Di Fan, Yannian Kou, and Chuanhou Gao. Causal disentangled representation learning with vae and causal flows.
- [29] Xinwei Shen, Furui Liu, Hanze Dong, Qing Lian, Zhitang Chen, and Tong Zhang. Weakly supervised disentangled generative causal representation learning. *Journal of Machine Learning Research*, 23(241):1–55, 2022.
- [30] Insu Jeon, Wonkwang Lee, Myeongjang Pyeon, and Gunhee Kim. Ib-gan: Disentangled representation learning with information bottleneck generative adversarial networks. In *Proceedings of the AAAI Conference on Artificial Intelligence*, volume 35, pages 7926–7934, 2021.
- [31] Tao Yang, Yuwang Wang, Cuiling Lan, Yan Lu, and Nanning Zheng. Vector-based representation is the key: A study on disentanglement and compositional generalization. *arXiv preprint arXiv:2305.18063*, 2023.
- [32] Xin Jin, Bohan Li, Baao Xie, Wenyao Zhang, Jinming Liu, Ziqiang Li, Tao Yang, and Wenjun Zeng. Closed-loop unsupervised representation disentanglement with  $\beta$ -vae distillation and diffusion probabilistic feedback. *arXiv preprint arXiv:2402.02346*, 2024.
- [33] Agisilaos Chartsias, Thomas Joyce, Giorgos Papanastasiou, Scott Semple, Michelle Williams, David E Newby, Rohan Dharmakumar, and Sotirios A Tsaftaris. Disentangled representation learning in cardiac image analysis. *Medical image analysis*, 58:101535, 2019.
- [34] Cosmin I Bercea, Benedikt Wiestler, Daniel Rueckert, and Shadi Albarqouni. Federated disentangled representation learning for unsupervised brain anomaly detection. *Nature Machine Intelligence*, 4(8):685–695, 2022.
- [35] Lianrui Zuo, Yihao Liu, Jerry L Prince, and Aaron Carass. An overview of disentangled representation learning for mr image harmonization. *Deep Learning for Medical Image Analysis*, pages 135–152, 2024.
- [36] Abel Gonzalez-Garcia, Joost Van De Weijer, and Yoshua Bengio. Image-to-image translation for cross-domain disentanglement. *Advances in neural information processing systems*, 31, 2018.
- [37] Hsin-Ying Lee, Hung-Yu Tseng, Jia-Bin Huang, Maneesh Singh, and Ming-Hsuan Yang. Diverse image-to-image translation via disentangled representations. In *Proceedings of the European conference on computer vision (ECCV)*, pages 35–51, 2018.
- [38] Boqiang Zhang, Hongtao Xie, Zuan Gao, and Yuxin Wang. Choose what you need: Disentangled representation learning for scene text recognition, removal and editing. *arXiv preprint arXiv:2405.04377*, 2024.

- [39] Piaopiao Yu, Jie Guo, Fan Huang, Cheng Zhou, Hongwei Che, Xiao Ling, and Yanwen Guo. Hierarchical disentangled representation learning for outdoor illumination estimation and editing. In *Proceedings of the IEEE/CVF International Conference on Computer Vision*, pages 15313–15322, 2021.
- [40] Baao Xie, Bohan Li, Zequn Zhang, Junting Dong, Xin Jin, Jingyu Yang, and Wenjun Zeng. Navinerf: Nerf-based 3d representation disentanglement by latent semantic navigation. In *Proceedings of the IEEE/CVF International Conference on Computer Vision*, pages 17992–18002, 2023.
- [41] Katja Schwarz, Yiyi Liao, Michael Niemeyer, and Andreas Geiger. Graf: Generative radiance fields for 3d-aware image synthesis. *Advances in Neural Information Processing Systems*, 33:20154–20166, 2020.
- [42] Michael Niemeyer and Andreas Geiger. Giraffe: Representing scenes as compositional generative neural feature fields. In *Proceedings of the IEEE/CVF Conference on Computer Vision and Pattern Recognition*, pages 11453–11464, 2021.
- [43] Hyunjik Kim and Andriy Mnih. Disentangling by factorising. In *International conference on machine learning*, pages 2649–2658. PMLR, 2018.
- [44] Minyoung Kim, Yuting Wang, Pritish Sahu, and Vladimir Pavlovic. Relevance factor vae: Learning and identifying disentangled factors. *arXiv preprint arXiv:1902.01568*, 2019.
- [45] Zihao Chen, Wenyong Wang, and Sai Zou. Break the spell of total correlation in betatcvae. *arXiv preprint arXiv:2210.08794*, 2022.
- [46] Karsten Roth, Mark Ibrahim, Zeynep Akata, Pascal Vincent, and Diane Bouchacourt. Disentanglement of correlated factors via hausdorff factorized support. *arXiv preprint arXiv:2210.07347*, 2022.
- [47] Yunhao Ge, Sami Abu-El-Haija, Gan Xin, and Laurent Itti. Zero-shot synthesis with group-supervised learning. *arXiv preprint arXiv:2009.06586*, 2020.
- [48] Matthew J Vowels, Necati Cihan Camgoz, and Richard Bowden. Gated variational autoencoders: Incorporating weak supervision to encourage disentanglement. In *2020 15th IEEE International Conference on Automatic Face and Gesture Recognition (FG 2020)*, pages 125–132. IEEE, 2020.
- [49] Diane Bouchacourt, Ryota Tomioka, and Sebastian Nowozin. Multi-level variational autoencoder: Learning disentangled representations from grouped observations. In *Proceedings of the AAAI Conference on Artificial Intelligence*, volume 32, 2018.
- [50] Attila Szabo, Qiyang Hu, Tiziano Portenier, Matthias Zwicker, and Paolo Favaro. Understanding degeneracies and ambiguities in attribute transfer. In *Proceedings of the European Conference on Computer Vision (ECCV)*, pages 700–714, 2018.
- [51] Andrew Ross and Finale Doshi-Velez. Benchmarks, algorithms, and metrics for hierarchical disentanglement. In *International Conference on Machine Learning*, pages 9084–9094. PMLR, 2021.
- [52] Xinyang Li, Shengchuan Zhang, Jie Hu, Liujuan Cao, Xiaopeng Hong, Xudong Mao, Feiyue Huang, Yongjian Wu, and Rongrong Ji. Image-to-image translation via hierarchical style disentanglement. In *Proceedings of the IEEE/CVF conference on computer vision and pattern recognition*, pages 8639–8648, 2021.
- [53] Wayne Xin Zhao, Kun Zhou, Junyi Li, Tianyi Tang, Xiaolei Wang, Yupeng Hou, Yingqian Min, Beichen Zhang, Junjie Zhang, Zican Dong, et al. A survey of large language models. *arXiv preprint arXiv:2303.18223*, 2023.
- [54] Alec Radford, Jong Wook Kim, Chris Hallacy, Aditya Ramesh, Gabriel Goh, Sandhini Agarwal, Girish Sastry, Amanda Askell, Pamela Mishkin, Jack Clark, et al. Learning transferable visual models from natural language supervision. In *International conference on machine learning*, pages 8748–8763. PMLR, 2021.
- [55] Bin Lin, Zhenyu Tang, Yang Ye, Jiayi Cui, Bin Zhu, Peng Jin, Junwu Zhang, Munan Ning, and Li Yuan. Moe-llava: Mixture of experts for large vision-language models. *arXiv preprint arXiv:2401.15947*, 2024.
- [56] Yuliang Liu, Biao Yang, Qiang Liu, Zhang Li, Zhiyin Ma, Shuo Zhang, and Xiang Bai. Textmonkey: An ocr-free large multimodal model for understanding document. *arXiv preprint arXiv:2403.04473*, 2024.
- [57] R OpenAI. Gpt-4 technical report. arxiv 2303.08774. *View in Article*, 2(5), 2023.
- [58] Gemini Team, Rohan Anil, Sebastian Borgeaud, Yonghui Wu, Jean-Baptiste Alayrac, Jiahui Yu, Radu Soricut, Johan Schalkwyk, Andrew M Dai, Anja Hauth, et al. Gemini: a family of highly capable multimodal models. *arXiv preprint arXiv:2312.11805*, 2023.

- [59] Yossi Gandelsman, Alexei A Efros, and Jacob Steinhardt. Interpreting clip’s image representation via text-based decomposition. *arXiv preprint arXiv:2310.05916*, 2023.
- [60] Zhengyuan Yang, Linjie Li, Kevin Lin, Jianfeng Wang, Chung-Ching Lin, Zicheng Liu, and Lijuan Wang. The dawn of lmms: preliminary explorations with gpt-4v (ision). arxiv. *arXiv preprint arXiv:2309.17421*, 2023.
- [61] Gpt-4v(ision) system card. 2023.
- [62] Hello, gpt-4o. *OpenAI*, 2025.
- [63] Maxim Enis and Mark Hopkins. From llm to nmt: Advancing low-resource machine translation with claude. *arXiv preprint arXiv:2404.13813*, 2024.
- [64] Shengqiong Wu, Hao Fei, Leigang Qu, Wei Ji, and Tat-Seng Chua. Next-gpt: Any-to-any multimodal llm. *arXiv preprint arXiv:2309.05519*, 2023.
- [65] Angus Yang, Zehan Li, and Jie Li. Advancing genai assisted programming—a comparative study on prompt efficiency and code quality between gpt-4 and glm-4. *arXiv preprint arXiv:2402.12782*, 2024.
- [66] Samyadeep Basu, Keivan Rezaei, Ryan Rossi, Cherry Zhao, Vlad Morariu, Varun Manjunatha, and Soheil Feizi. On mechanistic knowledge localization in text-to-image generative models. *arXiv preprint arXiv:2405.01008*, 2024.
- [67] Harshvardhan Sikka, Weishun Zhong, Jun Yin, and Cengiz Pehlevant. A closer look at disentangling in  $\beta$ -vae. In *2019 53rd Asilomar Conference on Signals, Systems, and Computers*, pages 888–895. IEEE, 2019.
- [68] Deokyun Kim, Minseon Kim, Gihyun Kwon, and Dae-Shik Kim. Progressive face super-resolution via attention to facial landmark. *arXiv preprint arXiv:1908.08239*, 2019.
- [69] Giuseppe Amato, Fabrizio Falchi, Claudio Gennaro, and Claudio Vairo. A comparison of face verification with facial landmarks and deep features. In *10th International Conference on Advances in Multimedia (MMEDIA)*, pages 1–6, 2018.
- [70] Martin Heusel, Hubert Ramsauer, Thomas Unterthiner, Bernhard Nessler, and Sepp Hochreiter. Gans trained by a two time-scale update rule converge to a local nash equilibrium. *Advances in neural information processing systems*, 30, 2017.
- [71] Robert H Somers. A new asymmetric measure of association for ordinal variables. *American sociological review*, pages 799–811, 1962.
- [72] Maurice G Kendall. A new measure of rank correlation. *Biometrika*, 30(1/2):81–93, 1938.
- [73] Yixin Liu, Yu Zheng, Daokun Zhang, Hongxu Chen, Hao Peng, and Shirui Pan. Towards unsupervised deep graph structure learning. In *Proceedings of the ACM Web Conference 2022*, pages 1392–1403, 2022.
- [74] Thomas N Kipf and Max Welling. Semi-supervised classification with graph convolutional networks. *arXiv preprint arXiv:1609.02907*, 2016.
- [75] Ziwei Liu, Ping Luo, Xiaogang Wang, and Xiaoou Tang. Deep learning face attributes in the wild. In *Proceedings of International Conference on Computer Vision (ICCV)*, December 2015.
- [76] Fisher Yu, Ari Seff, Yinda Zhang, Shuran Song, Thomas Funkhouser, and Jianxiong Xiao. Lsun: Construction of a large-scale image dataset using deep learning with humans in the loop. *arXiv preprint arXiv:1506.03365*, 2015.
- [77] Adam Paszke, Sam Gross, Soumith Chintala, Gregory Chanan, Edward Yang, Zachary DeVito, Zeming Lin, Alban Desmaison, Luca Antiga, and Adam Lerer. Automatic differentiation in pytorch. 2017.
- [78] Jonathan Ho, Ajay Jain, and Pieter Abbeel. Denoising diffusion probabilistic models. *Advances in neural information processing systems*, 33:6840–6851, 2020.
- [79] Keyu Tian, Yi Jiang, Zehuan Yuan, Bingyue Peng, and Liwei Wang. Visual autoregressive modeling: Scalable image generation via next-scale prediction. *arXiv preprint arXiv:2404.02905*, 2024.



## A Appendix

### A.1 Discussion

**Disentanglement Ability.** As shown in Table 3, we evaluate the disentanglement ability of our model (DRL branch only) against typical DRL models. Our model outperforms them across numerous metrics. However, it is really meaningful and interesting to discuss "what is a better disentanglement".

Table 3: Disentanglement metrics among VAE,  $\beta$ -VAE and GEM.

Models	MIG	IRS	MI	Info
VAE	0.19	0.35	0.84	0.81
$\beta$ -VAE	0.49	0.55	0.88	0.82
<b>GEM</b>	<b>0.53</b>	<b>0.60</b>	<b>0.86</b>	<b>0.85</b>

If it means the better performance on independently decomposing factors, then the inclusion of interrelations might not seem beneficial; however, if it refers to a better performance/practicality for real and complex scenarios, our disentanglement paradigm excels by statistically capturing the logical rules of real world. Specifically, the inclusion of interrelations can be beneficial in model generalizability, counterfactual reasoning and practical usages.

**Trade-off between Quality and Interpretability.** Even though our model achieved superior performance among DRL approaches, an inevitable trade-off between reconstruction and disentanglement remains, resulting in decreased reconstruction quality compared to the models focused on generation quality such as GANs and Diffusions (see Table 4).

Table 4: Quantitative comparison results with leading image generation models in FID and KID.

Method	CelebA (64×64)		CelebA (256×256)	
	FID ↓	KID ×10 <sup>3</sup> ↓	FID ↓	KID ×10 <sup>3</sup> ↓
<b>GEM (Ours)</b>	46.05	48.32	50.93	51.01
Vanilla VAE	53.39	51.48	56.82	61.26
StyleGAN2 (40k steps)	12.94	9.20	18.02	19.55
DDPM (Diffusion, $T = 1k$ )	8.56	<b>6.56</b>	15.93	10.01
DDIM (Implicit Diffusion, $T = 1k$ )	10.04	8.15	16.24	13.62
Stable Diffusion (fine-tuning)	<b>7.72</b>	7.22	<b>10.63</b>	<b>9.17</b>

Since our model is oriented towards interpretability, we consider this trade-off acceptable. However, it is insightful to leverage the advantages of both DRL and non-DRL models within a mutually beneficial closed-loop architecture, and we will make efforts to improve our work in this direction.

**Current Limitations.** Compared to existing DRL approaches, GEM emphasizes discovering underlying interrelations between attributes. This logical and effective framework can benefit a wide range of downstream tasks and practical applications such as controllable generation, medical image analysis, and automatic driving. However, there are still some limitations to this method. Firstly, the trade-off between reconstruction quality and disentanglement capacity, as a common challenge in the domain, is still not properly addressed in this work. To tackle it, we are currently investigating the integration of powerful generative models, e.g., diffusion models [78] and visual auto-regressive models [79], into our framework. Secondly, the current implementation of GEM is not designed to work with 3D data, where 3D representations are much more complex. To understand our real world, it would be necessary to enhance the model with specific improvements to handle 3D scenes.

### A.2 Dataset details

**CelebA.** The Celebrity Faces Attributes (CelebA) dataset [75] is a widely-used large-scale face attributes dataset that contains more than 200,000 celebrity images, each annotated with 40 attributes.

These annotations cover a wide range of facial attributes such as ‘smiling’, ‘wearing Hat’, ‘young’, ‘wavy Hair’, ‘male’, and ‘mustache’. These attributes are labeled as present or absent in each image. This dataset is designed for various DRL and computer vision tasks, such as face recognition, face attribute disentanglement, and face editing. Commonly, we use employ the entirety of the CelebA dataset, which includes 162,770 images for training, 19,867 for validation, and 19,962 for testing.

**LSUN.** The Large-scale Scene Understanding (LSUN) dataset [76] is a comprehensive collection for deep learning and computer vision, widely used in the domain of perceptual analysis and attribute disentanglement. This dataset consists of around one million labeled images for each of 10 scene categories and 20 object categories. The scene categories include diverse environments such as bedrooms, conference rooms, dining rooms, kitchens, living rooms, and etc. The object categories in LSUN include horse, car, church, etc. We select a typical subset, LSUN-horse, to demonstrate the model’s generalizability. We believe these two datasets are diverse enough to verify our GEM.

### A.3 Baseline details

#### A.3.1 $\beta$ -VAE

The  $\beta$ -VAE [15] is an extension of the standard VAE [14], introducing an adjustable hyperparameter  $\beta$  prior to the KL term in vanilla VAE:

$$\mathcal{L}(\theta, \phi) = \mathbb{E}_{q_\phi(\mathbf{z}|\mathbf{x})} [\log p_\theta(\mathbf{x}|\mathbf{z})] - \beta D_{KL}(q_\phi(\mathbf{z}|\mathbf{x}) \| p_\theta(\mathbf{z})) \quad (12)$$

where the penalty coefficient  $\beta$  balances the disentanglement capacity and reconstruction quality. When  $\beta > 1$ , this penalty increases the emphasis on learning disentangled representations in the latent space. However, increasing  $\beta$  can cause a trade-off on the reconstruction quality.

#### A.3.2 $\beta$ -TCVAE

The Total Correlation beta-VAE ( $\beta$ -TCVAE) [16] builds upon the  $\beta$ -VAE to further enhance the disentanglement of latent representations. It achieves this by the reduction of the total correlation (TC) term, extracted from the KL divergence term:

$$\mathbb{E}_{p(x)}[KL(q(z|x) \| p(z))] = KL(q(z,x) \| q(z)p(x)) + \beta KL\left(q(z) \| \prod_j q(z_j)\right) + \sum_j KL(q(z_j) \| p(z_j)) \quad (13)$$

where  $j$  represents the dimension of latent code  $z$ . The penalty coefficient  $\beta$  is selectively applied to the second term, i.e. TC term, on the right side of the loss function. It aims to make latent variables statistically independent of each other, therefore enhancing disentanglement. We include  $\beta$ -TCVAE in the quantitative comparisons, following the official implementation.

#### A.3.3 FactorVAE

The FactorVAE [43] is a typical variant of VAE, which employs a discriminator network in an adversarial manner to accurately estimate and minimize the total correlation term in the loss function. This adversarial strategy further enforces the factorization of the latent space, leading to improved disentanglement. We include  $\beta$ -VAE,  $\beta$ -TCVAE, FactorVAE in the quantitative comparisons following their official implementation. We evaluate the reconstruction quality by employing the Fréchet Inception Distance (FID) and Kernel Inception Distance (KID) metrics for comparative assessment.

#### A.3.4 DEAR

DEAR [29] is the weakly supervised structural disengagement framework. It facilitates causal representation learning by adopting a structural causal model (SCM) as the prior distribution. This SCM prior is supervised by the information on the ground-truth factors and their underlying causal structure from the database. We integrate DEAR into the quantitative and qualitative comparisons, training it with the annotations provided by the CelebA. All in all, we evaluate our unsupervised framework against both unsupervised ( $\beta$ -VAE,  $\beta$ -TCVAE, FactorVAE) and supervised (DEAR) DRL methods, thereby rigorously evaluating the capabilities in reconstruction and disentanglement.

### A.4 Face landmark results

Landmark detection are algorithm and technique utilized to detect and track specific key points in the image or video, encompassing a wide range of applications across various fields such as

computer vision, robotics, and geospatial analysis. In this work, we employ landmark detection as a pre-processing method to extract the key points of the main object, thus removing the redundant parts in the image through cropping and resizing.

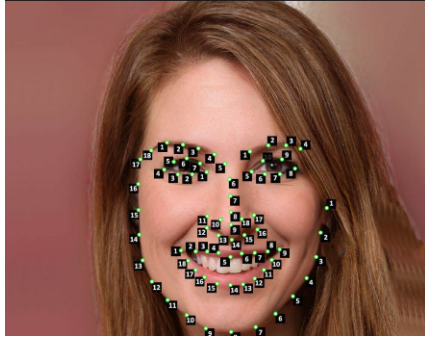


Figure 10: 68-points landmark pre-processing for data from the CelebA.

We introduce the pre-processing phase for CelebA, where 68 landmark points are identified and extracted commonly. As shown in Figure 10, points 1 to 17 present the jawline, points 18 to 27 for the eyebrows, points 28 to 36 for the nose, points 37-48 for the eyes, and points 49-68 identify the lips.

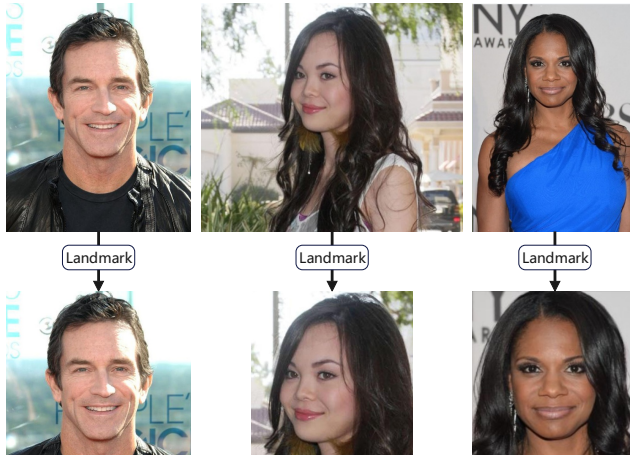


Figure 11: Image normalization based on the landmark detection.

Figure 11 illustrates some results of the pre-processing block. The normalized images benefit subsequent factor disentanglement and interrelation discovery.

### A.5 Details of adversarial training strategy

As described in Section 3.1, the prior assumption that  $p_\theta(z) \sim \mathcal{N}(0, 1)$  no longer holds, we reformulate the  $\beta$ -VAE loss as:

$$\begin{aligned} \mathcal{L}(\theta, \phi) &= \mathbb{E}_{x \sim q_\phi(x)} (\mathbb{E}_{z \sim q_\phi(z|x)} [\log p_\theta(x|z)] - \beta D_{KL}(q_\phi(z|x) \| p_\theta(z))) \\ &= \mathbb{E}_{x, z \sim q_\phi(z, x)} [\log p_\theta(x|z)] - \beta \mathbb{E}_{x, z \sim q_\phi(z, x)} \log \left( \frac{q_\phi(z|x)}{p_\theta(z)} \right) \end{aligned} \quad (14)$$

Subsequently, the gradient of  $\mathcal{L}$  with respect to  $\theta$  can be derived as:

$$\begin{aligned}
\nabla_{\theta} \mathcal{L}(\theta, \phi) &\stackrel{x=D_{\theta}(z)}{=} \mathbb{E}_{z \sim q(z)} [\nabla_x \log(p_{\theta}(x|z)) \nabla_{\theta} x - \beta \nabla_x \log(q_{\phi}(z|x)/p_{\theta}(z)) \nabla_{\theta} x] \\
&= \mathbb{E}_{z \sim q(z)} \nabla_x [\log(p_{\theta}(x|z)) - \beta \log(\frac{q_{\phi}(z|x)}{p_{\theta}(z)})] \nabla_{\theta} x \\
&= \mathbb{E}_{z \sim q(z)} \nabla_x [\log(p_{\theta}(x, z)) - \beta \log(\frac{q_{\phi}(z, x)}{q_{\phi}(x)})] \nabla_{\theta} x \\
&= \mathbb{E}_{z \sim q(z)} \nabla_x [\log(p_{\theta}(x, z)) - \beta \log(\frac{q_{\phi}(z, x)}{q_{\phi}(x)})] \nabla_{\theta} x \\
&= \mathbb{E}_{z \sim q(z)} \nabla_x [\log(\frac{p_{\theta}(x, z)}{\beta q_{\phi}(x, z)})] \nabla_{\theta} x + \beta \mathbb{E}_{z \sim q(z)} \nabla_x q_{\phi}(x) \nabla_{\theta} x
\end{aligned} \tag{15}$$

where the first term on the right side needs to be approximated by a neural network due to the altered assumption. Therefore, we define:

$$\begin{aligned}
p(x, z) &= p((x, z) \in E_{\phi})p(x, z|(x, z) \in E_{\phi}) + p((x, z) \in D_{\theta})p(x, z|(x, z) \in D_{\theta}) \\
&= p((x, z) \in E_{\phi})q_{\phi}(x, z) + p((x, z) \in D_{\theta})p_{\theta}(x, z)
\end{aligned} \tag{16}$$

then

$$\begin{aligned}
p((x, z) \in E_{\phi}|x, z) &= \frac{p((x, z) \in E_{\phi})p(x, z|(x, z) \in E_{\phi})}{p(x, z)} \\
&= \frac{1}{1 + \alpha \frac{q_{\phi}(x, z)}{p_{\theta}(x, z)}} \\
p((x, z) \in D_{\theta}|x, z) &= \frac{p((x, z) \in D_{\theta})p(x, z|(x, z) \in D_{\theta})}{p(x, z)} \\
&= \frac{1}{1 + \frac{1}{\alpha} \frac{p_{\theta}(x, z)}{q_{\phi}(x, z)}} \\
\alpha &= \frac{p((x, z) \in D_{\theta})}{p((x, z) \in E_{\phi})}
\end{aligned} \tag{17}$$

Given the controllable proportion of the input images, denoted by  $\alpha \in [0, 1]$ , we define:

$$D(x, y) = \log\left(\frac{p_{\theta}(x, z)}{\beta q_{\phi}(x, z)}\right) \tag{18}$$

then

$$\frac{p_{\theta}(x, z)}{\beta q_{\phi}(x, z)} = e^{D(x, z)} \tag{19}$$

where  $\beta \in (1, +\infty)$  is proposed to enhance the disentanglement ability of  $\beta$ -VAE. We subsequently define the variable  $k$ :

$$\text{suppose } k = \frac{\alpha}{\beta}$$

$$\begin{aligned}
p((x, z) \in E_{\phi}|x, z) &= \frac{1}{1 + k e^{-D(x, z)}} \\
p((x, z) \in D_{\theta}|x, z) &= \frac{1}{1 + \frac{1}{k} e^{D(x, z)}}
\end{aligned} \tag{20}$$

$$\text{since : } 1 = p((x, z) \in E_{\phi}|x, z) + p((x, z) \in D_{\theta}|x, z)$$

Given that the solution for  $k$  is determined to be 1, under the condition that  $\alpha = \beta = 1$  (otherwise  $\forall(x, z) D(x, z) = 0$  which is obviously impossible), it is logically imperative to require distribution  $p(x, z|(x, z) \in E_{\phi})$  and  $p(x, y|(x, z) \in D_{\theta})$  to closely approximate  $p(x, z)$ . On this basis, we found:

$$\begin{aligned}
p(x, z) = p(x, z | (x, z) \in E_\phi) &\iff p((x, z) \in E_\phi | x, z) = p((x, z) \in E_\phi) \\
p(x, z) = p(x, z | (x, z) \in D_\theta) &\iff p((x, z) \in D_\theta | x, z) = p((x, z) \in D_\theta)
\end{aligned} \tag{21}$$

where if  $\alpha = 1$ , we attain the optimization objective of  $p((x, y) \in D_\theta) = p((x, y) \in E_\phi) = \frac{1}{N_m}$ . To this end, we can finally use the cross-entropy algorithm to optimize  $D$ :

$$\begin{aligned}
\mathcal{L}_{adv} &= \mathcal{L}(D) = \text{cross\_entropy}(p_{gt}, p_{\theta, \phi}) \\
&= -\frac{1}{N_{bc}} \sum_{i=0}^{N_{bc}} [p((x_i, z_i) \in E_\phi) \log p((x_i, z_i) \in E_\phi | x, z) + p((x_i, z_i) \in D_\theta) \log p((x_i, z_i) \in D_\theta | x, z)] \\
&= -\frac{1}{N_{bc} N_m} \sum_{i=0}^{N_{bc}} [-\text{softplus}(-D(x_i, z_i)) - \text{softplus}(D(x_i, z_i))] \\
&= \frac{1}{N_{bc} N_m} \sum_{i=0}^{N_{bc}} [\text{softplus}(-D(x_i, z_i)) + \text{softplus}(D(x_i, z_i))] \\
&= \frac{1}{N_{bc} N_m} \left[ \sum_{i=0; (x_i, z_i) \in E_\phi}^{N_{bc}} \text{softplus}(-D(x_i, z_i)) + \sum_{i=0; (x_i, z_i) \in D_\theta}^{N_{bc}} \text{softplus}(D(x_i, z_i)) \right],
\end{aligned} \tag{22}$$

where  $\text{softplus}(x) = \ln(1 + e^x)$  is a smooth activation function.  $N_{bc}$  and  $N_m$  represent the number of samples and posterior samples in a batch. The additional adversarial loss ensures the maintenance of reconstruction quality, tending to diminish as the capacity for disentanglement increases.

## A.6 Details of interrelation determining strategy

In the interrelation discovery branch, we propose the Somers' Delta (Somers' D) [71] algorithm to determine and rank the bidirectional relations among the attributes extracted by the  $\beta$ -VAE branch. Somers' D is a statistical measure used to assess the strength and direction of the relation between variables. It is a nonparametric measure that can be considered a measure of rank correlation, similar to Kendall's tau [72], but with a focus on asymmetric relations.

Specifically, the calculation of impact scores based on Somers' D is upon the number of concordant pairs ( $C$ ) and discordant pairs ( $D$ ). The formula of Somers' D on variable  $Y$  and  $X$  can be given as:

$$D_{YX} = \frac{C - D}{C + D + T_x}, \quad D_{XY} = \frac{C - D}{C + D + T_y} \tag{23}$$

where  $T_x$  is the number of ties only for the independent variable  $X$ , and  $T_y$  is the number of ties only for the independent variable  $Y$ . The obtained attribute scores and interrelations from MLLMs are evaluated. For example, suppose we have the sample dataset  $S = (1,2), (3,1), (2,3)$ :

Variable	Pairs	Value
$N_c$	(1,2) vs (2,3)	1
$N_d$	(1,2) vs (3,1) and (2,3) vs (3,1)	2
$N_y$	None	0

Then the Somers' D indicator can be calculated as follows:

$$D = \frac{N_c - N_d}{N_c + N_d + T_y} = \frac{1 - 2}{1 + 2 + 0} = -\frac{1}{3} \tag{24}$$

This obtains a value of approximately -0.33, signifying a negative correlation between variables  $X$  and  $Y$ . This calculation demonstrates that the Somers' D metric is straightforward to calculate and



is particularly applicable to ordinal variables. Furthermore, Somers' D is asymmetric and capable of distinguishing bidirectional relationships between variables. These characteristics make it highly suitable for integration into our model.

### A.7 Additional results

We perform additional evaluation results for individual attributes on different MLLMs with Ground Truth (GT) labels in CelebA. As shown in Figure 12, the results demonstrate the reliability of the GPT-4o employed in our work.

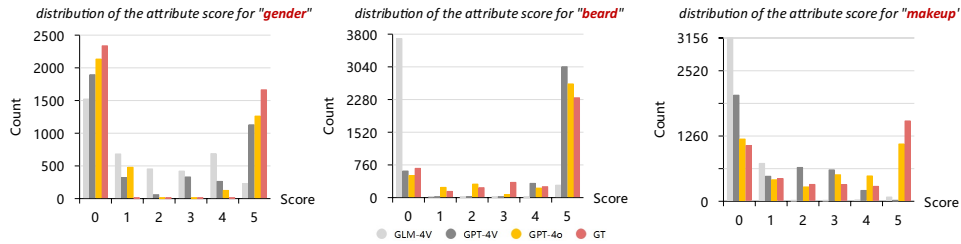


Figure 12: Reconstruction results of the CelebA.

We also present additional results that demonstrate the capacity of GEM in fine-grained and relation-aware disentanglement. Figure 13, Figure 14, Figure 15 demonstrates the reconstruction results on the CelebA, LSUN-bedroom and LSUN-horse, respectively. It is obvious that following the landmark pre-processing, GEM effectively identify the main part of facial images while mitigating noise. This enhancement facilitates the downstream processes of the model. In addition, as depicted in Figure 16, GEM is capable of processing high-definition images given sufficient computational resources.



Figure 13: Reconstruction results of the CelebA.

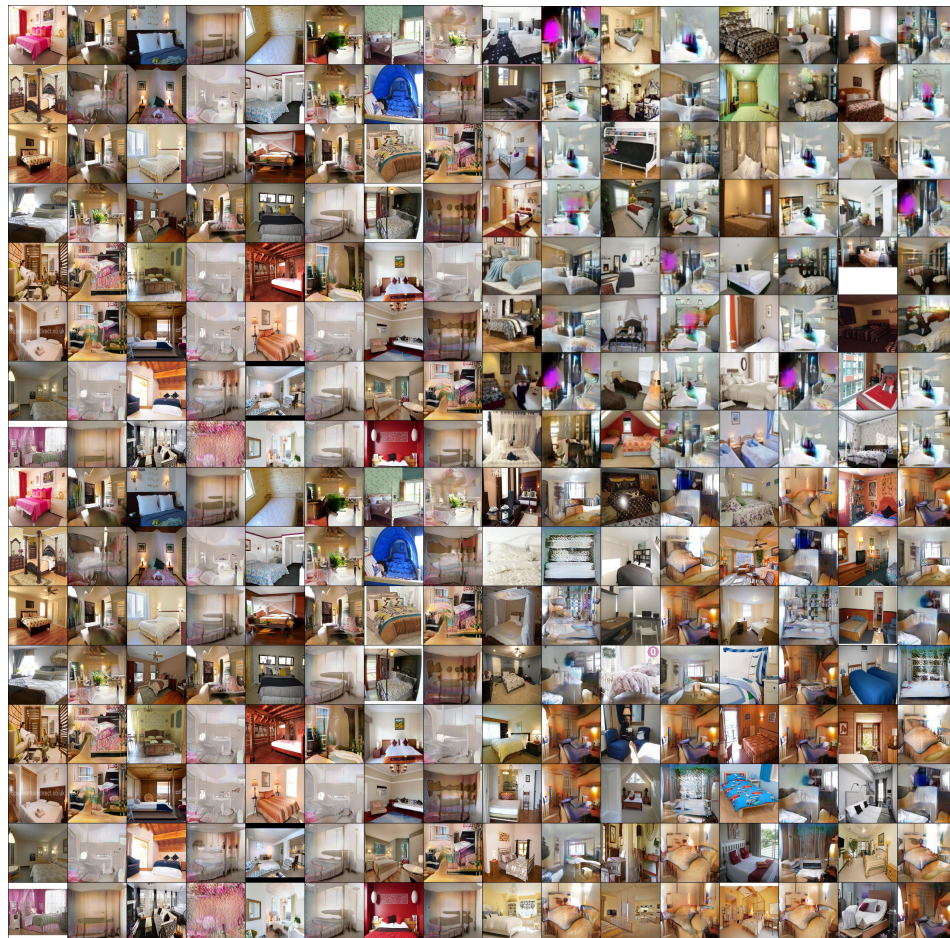


Figure 14: Reconstruction results of the LSUN-bedroom.





Figure 15: Reconstruction results of the LSUN-horse.



Figure 16: high-definition results at  $256 \times 256$  on the CebeA.

## NeurIPS Paper Checklist

### 1. Claims

Question: Do the main claims made in the abstract and introduction accurately reflect the paper's contributions and scope?

Answer: [Yes]

Justification: We clearly claim the contribution and scope in the abstract and introduction, substantiated by theoretical and experimental results.

Guidelines:

- The answer NA means that the abstract and introduction do not include the claims made in the paper.
- The abstract and/or introduction should clearly state the claims made, including the contributions made in the paper and important assumptions and limitations. A No or NA answer to this question will not be perceived well by the reviewers.
- The claims made should match theoretical and experimental results, and reflect how much the results can be expected to generalize to other settings.
- It is fine to include aspirational goals as motivation as long as it is clear that these goals are not attained by the paper.

### 2. Limitations

Question: Does the paper discuss the limitations of the work performed by the authors?

Answer: [Yes]

Justification: Limitations and future work are discussed in Appendix A.1, which will be included in the camera-ready version.

Guidelines:

- The answer NA means that the paper has no limitation while the answer No means that the paper has limitations, but those are not discussed in the paper.
- The authors are encouraged to create a separate "Limitations" section in their paper.
- The paper should point out any strong assumptions and how robust the results are to violations of these assumptions (e.g., independence assumptions, noiseless settings, model well-specification, asymptotic approximations only holding locally). The authors should reflect on how these assumptions might be violated in practice and what the implications would be.
- The authors should reflect on the scope of the claims made, e.g., if the approach was only tested on a few datasets or with a few runs. In general, empirical results often depend on implicit assumptions, which should be articulated.
- The authors should reflect on the factors that influence the performance of the approach. For example, a facial recognition algorithm may perform poorly when image resolution is low or images are taken in low lighting. Or a speech-to-text system might not be used reliably to provide closed captions for online lectures because it fails to handle technical jargon.
- The authors should discuss the computational efficiency of the proposed algorithms and how they scale with dataset size.
- If applicable, the authors should discuss possible limitations of their approach to address problems of privacy and fairness.
- While the authors might fear that complete honesty about limitations might be used by reviewers as grounds for rejection, a worse outcome might be that reviewers discover limitations that aren't acknowledged in the paper. The authors should use their best judgment and recognize that individual actions in favor of transparency play an important role in developing norms that preserve the integrity of the community. Reviewers will be specifically instructed to not penalize honesty concerning limitations.

### 3. Theory Assumptions and Proofs

Question: For each theoretical result, does the paper provide the full set of assumptions and a complete (and correct) proof?



Answer: [Yes]

Justification: All the theoretical statements, theories and assumptions related to this work are referenced. The proofs and derivations of formulas in the paper are clearly stated in Section 3 and Appendix A.5.

Guidelines:

- The answer NA means that the paper does not include theoretical results.
- All the theorems, formulas, and proofs in the paper should be numbered and cross-referenced.
- All assumptions should be clearly stated or referenced in the statement of any theorems.
- The proofs can either appear in the main paper or the supplemental material, but if they appear in the supplemental material, the authors are encouraged to provide a short proof sketch to provide intuition.
- Inversely, any informal proof provided in the core of the paper should be complemented by formal proofs provided in appendix or supplemental material.
- Theorems and Lemmas that the proof relies upon should be properly referenced.

#### 4. Experimental Result Reproducibility

Question: Does the paper fully disclose all the information needed to reproduce the main experimental results of the paper to the extent that it affects the main claims and/or conclusions of the paper (regardless of whether the code and data are provided or not)?

Answer: [Yes]

Justification: We are committed to ensuring the reproducibility of this study. The project will be open-sourced, and comprehensive details for reproducibility can be found in Section 4.

Guidelines:

- The answer NA means that the paper does not include experiments.
- If the paper includes experiments, a No answer to this question will not be perceived well by the reviewers: Making the paper reproducible is important, regardless of whether the code and data are provided or not.
- If the contribution is a dataset and/or model, the authors should describe the steps taken to make their results reproducible or verifiable.
- Depending on the contribution, reproducibility can be accomplished in various ways. For example, if the contribution is a novel architecture, describing the architecture fully might suffice, or if the contribution is a specific model and empirical evaluation, it may be necessary to either make it possible for others to replicate the model with the same dataset, or provide access to the model. In general, releasing code and data is often one good way to accomplish this, but reproducibility can also be provided via detailed instructions for how to replicate the results, access to a hosted model (e.g., in the case of a large language model), releasing of a model checkpoint, or other means that are appropriate to the research performed.
- While NeurIPS does not require releasing code, the conference does require all submissions to provide some reasonable avenue for reproducibility, which may depend on the nature of the contribution. For example
  - (a) If the contribution is primarily a new algorithm, the paper should make it clear how to reproduce that algorithm.
  - (b) If the contribution is primarily a new model architecture, the paper should describe the architecture clearly and fully.
  - (c) If the contribution is a new model (e.g., a large language model), then there should either be a way to access this model for reproducing the results or a way to reproduce the model (e.g., with an open-source dataset or instructions for how to construct the dataset).
  - (d) We recognize that reproducibility may be tricky in some cases, in which case authors are welcome to describe the particular way they provide for reproducibility. In the case of closed-source models, it may be that access to the model is limited in some way (e.g., to registered users), but it should be possible for other researchers to have some path to reproducing or verifying the results.

## 5. Open access to data and code

Question: Does the paper provide open access to the data and code, with sufficient instructions to faithfully reproduce the main experimental results, as described in supplemental material?

Answer: [Yes]

Justification: The codes will be released in the camera-ready version, with detailed instructions for user to reproduce.

Guidelines:

- The answer NA means that paper does not include experiments requiring code.
- Please see the NeurIPS code and data submission guidelines (<https://nips.cc/public/guides/CodeSubmissionPolicy>) for more details.
- While we encourage the release of code and data, we understand that this might not be possible, so “No” is an acceptable answer. Papers cannot be rejected simply for not including code, unless this is central to the contribution (e.g., for a new open-source benchmark).
- The instructions should contain the exact command and environment needed to run to reproduce the results. See the NeurIPS code and data submission guidelines (<https://nips.cc/public/guides/CodeSubmissionPolicy>) for more details.
- The authors should provide instructions on data access and preparation, including how to access the raw data, pre-processed data, intermediate data, and generated data, etc.
- The authors should provide scripts to reproduce all experimental results for the new proposed method and baselines. If only a subset of experiments are reproducible, they should state which ones are omitted from the script and why.
- At submission time, to preserve anonymity, the authors should release anonymized versions (if applicable).
- Providing as much information as possible in supplemental material (appended to the paper) is recommended, but including URLs to data and code is permitted.

## 6. Experimental Setting/Details

Question: Does the paper specify all the training and test details (e.g., data splits, hyper-parameters, how they were chosen, type of optimizer, etc.) necessary to understand the results?

Answer: [Yes]

Justification: The experimental settings for our model, baseline, datasets and MLLMs can be found in Section 4 and Appendix A.2, A.4.

Guidelines:

- The answer NA means that the paper does not include experiments.
- The experimental setting should be presented in the core of the paper to a level of detail that is necessary to appreciate the results and make sense of them.
- The full details can be provided either with the code, in appendix, or as supplemental material.

## 7. Experiment Statistical Significance

Question: Does the paper report error bars suitably and correctly defined or other appropriate information about the statistical significance of the experiments?

Answer: [Yes]

Justification: The results of quantitative comparisons presented in this paper are accompanied by errors bar to achieve statistical significance (see Section 4.2).

Guidelines:

- The answer NA means that the paper does not include experiments.
- The authors should answer "Yes" if the results are accompanied by error bars, confidence intervals, or statistical significance tests, at least for the experiments that support the main claims of the paper.

- The factors of variability that the error bars are capturing should be clearly stated (for example, train/test split, initialization, random drawing of some parameter, or overall run with given experimental conditions).
- The method for calculating the error bars should be explained (closed form formula, call to a library function, bootstrap, etc.)
- The assumptions made should be given (e.g., Normally distributed errors).
- It should be clear whether the error bar is the standard deviation or the standard error of the mean.
- It is OK to report 1-sigma error bars, but one should state it. The authors should preferably report a 2-sigma error bar than state that they have a 96% CI, if the hypothesis of Normality of errors is not verified.
- For asymmetric distributions, the authors should be careful not to show in tables or figures symmetric error bars that would yield results that are out of range (e.g., negative error rates).
- If error bars are reported in tables or plots, The authors should explain in the text how they were calculated and reference the corresponding figures or tables in the text.

## 8. Experiments Compute Resources

Question: For each experiment, does the paper provide sufficient information on the computer resources (type of compute workers, memory, time of execution) needed to reproduce the experiments?

Answer: [Yes]

Justification: The computational efficiency of our framework is reported and compared with typical DRL models (see Section 4.2).

Guidelines:

- The answer NA means that the paper does not include experiments.
- The paper should indicate the type of compute workers CPU or GPU, internal cluster, or cloud provider, including relevant memory and storage.
- The paper should provide the amount of compute required for each of the individual experimental runs as well as estimate the total compute.
- The paper should disclose whether the full research project required more compute than the experiments reported in the paper (e.g., preliminary or failed experiments that didn't make it into the paper).

## 9. Code Of Ethics

Question: Does the research conducted in the paper conform, in every respect, with the NeurIPS Code of Ethics <https://neurips.cc/public/EthicsGuidelines?>

Answer: [Yes]

Justification: To our best knowledge, this study does not involve any ethical issues.

Guidelines:

- The answer NA means that the authors have not reviewed the NeurIPS Code of Ethics.
- If the authors answer No, they should explain the special circumstances that require a deviation from the Code of Ethics.
- The authors should make sure to preserve anonymity (e.g., if there is a special consideration due to laws or regulations in their jurisdiction).

## 10. Broader Impacts

Question: Does the paper discuss both potential positive societal impacts and negative societal impacts of the work performed?

Answer: [Yes]

Justification: The potential positive societal impacts are discussed in the paper and Appendix A.1, which will be included in the camera-ready version. To our best knowledge, this work does not cause any negative societal impacts.

Guidelines:

- The answer NA means that there is no societal impact of the work performed.
- If the authors answer NA or No, they should explain why their work has no societal impact or why the paper does not address societal impact.
- Examples of negative societal impacts include potential malicious or unintended uses (e.g., disinformation, generating fake profiles, surveillance), fairness considerations (e.g., deployment of technologies that could make decisions that unfairly impact specific groups), privacy considerations, and security considerations.
- The conference expects that many papers will be foundational research and not tied to particular applications, let alone deployments. However, if there is a direct path to any negative applications, the authors should point it out. For example, it is legitimate to point out that an improvement in the quality of generative models could be used to generate deepfakes for disinformation. On the other hand, it is not needed to point out that a generic algorithm for optimizing neural networks could enable people to train models that generate Deepfakes faster.
- The authors should consider possible harms that could arise when the technology is being used as intended and functioning correctly, harms that could arise when the technology is being used as intended but gives incorrect results, and harms following from (intentional or unintentional) misuse of the technology.
- If there are negative societal impacts, the authors could also discuss possible mitigation strategies (e.g., gated release of models, providing defenses in addition to attacks, mechanisms for monitoring misuse, mechanisms to monitor how a system learns from feedback over time, improving the efficiency and accessibility of ML).

#### 11. Safeguards

Question: Does the paper describe safeguards that have been put in place for responsible release of data or models that have a high risk for misuse (e.g., pretrained language models, image generators, or scraped datasets)?

Answer: [\[Yes\]](#)

Justification: Our framework rely on the VAE model, MLLMs and GNN model, so our safeguards are the same as theirs. To the best of our knowledge, these models poses no risks on misuse or dual-use.

Guidelines:

- The answer NA means that the paper poses no such risks.
- Released models that have a high risk for misuse or dual-use should be released with necessary safeguards to allow for controlled use of the model, for example by requiring that users adhere to usage guidelines or restrictions to access the model or implementing safety filters.
- Datasets that have been scraped from the Internet could pose safety risks. The authors should describe how they avoided releasing unsafe images.
- We recognize that providing effective safeguards is challenging, and many papers do not require this, but we encourage authors to take this into account and make a best faith effort.

#### 12. Licenses for existing assets

Question: Are the creators or original owners of assets (e.g., code, data, models), used in the paper, properly credited and are the license and terms of use explicitly mentioned and properly respected?

Answer: [\[Yes\]](#)

Justification: All the public baselines and datasets used in this paper are properly credited (see Section 4).

Guidelines:

- The answer NA means that the paper does not use existing assets.
- The authors should cite the original paper that produced the code package or dataset.
- The authors should state which version of the asset is used and, if possible, include a URL.

- The name of the license (e.g., CC-BY 4.0) should be included for each asset.
- For scraped data from a particular source (e.g., website), the copyright and terms of service of that source should be provided.
- If assets are released, the license, copyright information, and terms of use in the package should be provided. For popular datasets, [paperswithcode.com/datasets](https://paperswithcode.com/datasets) has curated licenses for some datasets. Their licensing guide can help determine the license of a dataset.
- For existing datasets that are re-packaged, both the original license and the license of the derived asset (if it has changed) should be provided.
- If this information is not available online, the authors are encouraged to reach out to the asset's creators.

### 13. **New Assets**

Question: Are new assets introduced in the paper well documented and is the documentation provided alongside the assets?

Answer: [Yes]

Justification: The assets of this project, primarily the codes, are well documented and will be released in the camera ready version.

Guidelines:

- The answer NA means that the paper does not release new assets.
- Researchers should communicate the details of the dataset/code/model as part of their submissions via structured templates. This includes details about training, license, limitations, etc.
- The paper should discuss whether and how consent was obtained from people whose asset is used.
- At submission time, remember to anonymize your assets (if applicable). You can either create an anonymized URL or include an anonymized zip file.

### 14. **Crowdsourcing and Research with Human Subjects**

Question: For crowdsourcing experiments and research with human subjects, does the paper include the full text of instructions given to participants and screenshots, if applicable, as well as details about compensation (if any)?

Answer: [NA]

Justification: The research presented in the paper exclusively utilizes public datasets and does not involve any crowdsourcing or research with human subjects.

Guidelines:

- The answer NA means that the paper does not involve crowdsourcing nor research with human subjects.
- Including this information in the supplemental material is fine, but if the main contribution of the paper involves human subjects, then as much detail as possible should be included in the main paper.
- According to the NeurIPS Code of Ethics, workers involved in data collection, curation, or other labor should be paid at least the minimum wage in the country of the data collector.

### 15. **Institutional Review Board (IRB) Approvals or Equivalent for Research with Human Subjects**

Question: Does the paper describe potential risks incurred by study participants, whether such risks were disclosed to the subjects, and whether Institutional Review Board (IRB) approvals (or an equivalent approval/review based on the requirements of your country or institution) were obtained?

Answer: [NA]

Justification: This paper does not involve crowdsourcing nor research with human subjects.

Guidelines:

- The answer NA means that the paper does not involve crowdsourcing nor research with human subjects.
- Depending on the country in which research is conducted, IRB approval (or equivalent) may be required for any human subjects research. If you obtained IRB approval, you should clearly state this in the paper.
- We recognize that the procedures for this may vary significantly between institutions and locations, and we expect authors to adhere to the NeurIPS Code of Ethics and the guidelines for their institution.
- For initial submissions, do not include any information that would break anonymity (if applicable), such as the institution conducting the review.